Heart Failure Reviews (2019) 24:759–777
https://doi.org/10.1007/s10741-019-09783-4

Surgical and physiological challenges in the development of left and right heart failure in rat models

Michael G. Katz[1] · Anthony S. Fargnoli[1] · Sarah M. Gubara[1] · Elena Chepurko[1] · Charles R. Bridges[1] · Roger J. Hajjar[1]

Published online: 22 March 2019

Abstract

Rodent surgical animal models of heart failure (HF) are critically important for understanding the proof of principle of the cellular alterations underlying the development of the disease as well as evaluating therapeutics. Robust, reproducible rodent models are a prerequisite to the development of pharmacological and molecular strategies for the treatment of HF in patients. Due to the absence of standardized guidelines regarding surgical technique and clear criteria for HF progression in rats, objectivity is compromised. Scientific publications in rats rarely fully disclose the actual surgical details, and technical and physiological challenges. This lack of reporting is one of the main reasons that the outcomes specified in similar studies are highly variable and associated with unnecessary loss of animals, compromising scientific assessment. This review details rat circulatory and coronary arteries anatomy, the surgical details of rat models that recreate the HF phenotype of myocardial infarction, ischemia/reperfusion, left and right ventricular pressure, and volume overload states, and summarizes the technical and physiological challenges of creating HF. The purpose of this article is to help investigators understand the underlying issues of current HF models in order to reduce variable results and ensure successful, reproducible models of HF.

Keywords Rat heart anatomy and physiology · Right heart failure · Left heart failure · Surgical models

Abbreviations

HF	Heart failure
LAD	Left anterior descending artery
ECG	Echocardiography
MI	Myocardial infarction
I/R	Ischemia–reperfusion
LV	Left ventricle
MRI	Magnetic resonance imaging
VT	Ventricular tachycardia
VF	Ventricular fibrillation
TAC	Transverse aortic constriction
AAC	Ascending aortic constriction
PA	Pulmonary artery
RV	Right ventricle
IVC	Inferior vena cava
AR	Aortic regurgitation
Qp	Pulmonary blood flow
Qs	Systemic blood flow

✉ Michael G. Katz
Michael.Katz1@mssm.edu

[1] Cardiovascular Research Center, Department of Cardiology, Icahn School of Medicine at Mount Sinai, 1470 Madison Ave., Box 1030, New York, NY 10029-6574, USA

Introduction

Significant contributions have been made to understand the pathophysiologic and genetic alterations in various animal models of heart failure (HF). Discovery of new molecular targets in animals allows researchers to formulate clinical treatments for HF, which can be potentially translated to human patients. Despite differences in cardiac physiology, anatomy, and molecular profile with respect to humans, rodents remain the fundamental for proof-of-concept studies testing HF phenotype and outcome. Rodent models used for translational studies in HF have led to the establishment of numerous new cellular and genetic methodologies and discovery of molecular pathways, which are successfully used in the clinic today. Most research studies preference rodent models due to a number of technical and economic considerations, namely (1) established housing protocols and low maintenance costs; thus, a large sample size can be studied in a relatively short time period, and a limited number of personnel are required;

(2) advances in both invasive catheter design and non-invasive micro-technology specifically for small-animal characterization that make assessment of heart function accurate and easily feasible; and (3) the basic experimentally induced heart failure models are accepted by the majority of researchers [1, 2].

In recent years, mice have been the most used species in cardiovascular research due to availability of transgenic and knockout mouse strains. Yet, investigators prefer to use rats for research studies involving complex surgical procedures like heart transplantation, creation of HF with various systemic arterio-venous shunts techniques, and the use of cardiopulmonary bypass because they are technically much easier in rats than in mice [3, 4]. However, scientific publications in rats rarely share the actual surgical details and technical and physiological challenges of HF creation [5–9]. A lack of description of standardized surgical technique and surgical guidelines is one of the main reasons that study outcomes are highly variable and associated with unnecessary loss of animals. This review has summarized the most frequently used rat models of left and right heart failure with a focus on highlighting and disclosing the essential surgical techniques and challenges.

Understanding rat heart anatomy and physiology

Rats are mammals and belong to the rodent superfamily *Muroidea*. The cardiac, pulmonary, and systemic circulatory systems and valves of the rat are similar to those of humans. The heart of a rat consists of four chambers. The brachiocephalic trunk is on the right side of the aortic arch and divides into the right common carotid artery and the right subclavian artery (Fig. 1). At the anterior part of the aortic arch is the left common carotid artery, and to the left of it, the left subclavian artery is readily identifiable [10, 11]. Additionally, the right and left atria have an extra coronary blood supply from internal mammary arteries [11]. The rat also has no true equivalent of a circumflex artery beside a small artery like ramus intermediate.

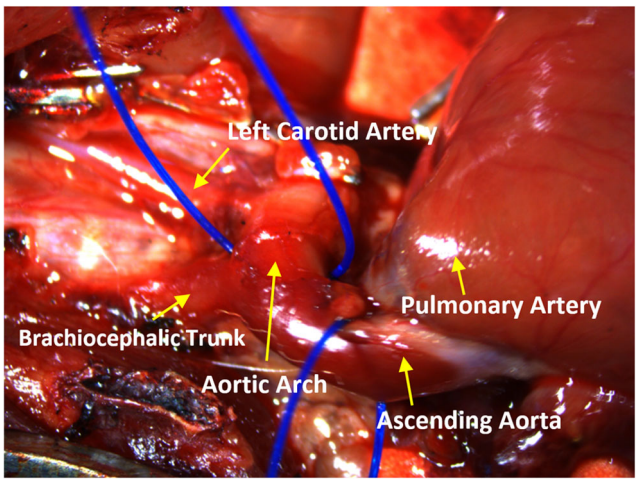

Fig. 1 Rat aortic anatomy. The figure demonstrates rat aorta anatomy. The ascending aorta leads to the aortic arch. The vessels of the aortic arch include the brachiocephalic trunk, which branches into the right carotid and right subclavian arteries, and the left carotid artery

A rat's heart rate is approximately five times higher in comparison to humans and the relationship between myocardial force and frequency is inversely proportional. Rat myocardium differs from human myocardium in that it has a shorter action potential without a plateau phase during contraction. It is well known that the duration of cardiac action potentials increases with body size and is approximately 50 ms in rat ventricles compared to 250 ms in humans. The physiology of action potential reflects the contribution of depolarizing and repolarizing currents. This contribution of ion channels is different between humans and rats. In rat ventricular muscle, the presence of a relatively large depolarization current activated outwardly rapidly brings the membrane potential back to a negative diastolic value. Thus, the rat ventricular myocyte action potential lacks a prominent plateau phase, resulting in a shorter duration action potential [12, 13]. Another difference is the mechanism of removal of calcium from the cytosol, and the activity of the sarcoplasmic reticulum (SR) calcium pump [14]. A study investigating SR Ca^{2+} uptake and Ca^{2+} leak in human cardiac muscle showed that (i) the maximum SR Ca^{2+} uptake is closely related to the measured SR Ca^{2+}-ATPase activity and the translocation of Ca^{2+} ions, (ii) the Ca^{2+} sensitivity of Ca^{2+}uptake is significantly higher in different human myofilaments, and (iii) SR Ca^{2+} leak rates in human myocardium are lower than those in rat heart and seemingly less affected by cytoplasmic adenosine diphosphate suggesting that SERCA regulation differs in the two species [15].

The most fundamental research studies utilizing rats involve the creation of myocardial infarct (MI) or ischemia/reperfusion in the left anterior descending (LAD) artery area [16–19]. The LAD artery in rats branches off the ascending aorta and transverses down over the anterior lateral wall of the left ventricle parallel to the interventricular groove. The septal artery is the first large arterial branch of the LAD. The other branches include several diagonals that supply the LV lateral and posterior free wall and pulmonary trunk. The most important surgical detail is that the LAD artery, through its course length to the apex, transverses completely intramurally [20]. Therefore, any external inspection is difficult. This important detail requires that the surgeon use cardiac landmarks, such as the left margin of the pulmonary trunk and left atrial appendage, to assure consistent results from the occlusion or ligation of the LAD. The proximal part of the LAD artery is usually located between these landmarks, close to the pulmonary artery. Since there is little collateral flow, inter-arterial

anastomoses are rare in the rat [10, 11]. Permanent ligation of the LAD artery results in a consistent, large, and uniform ischemic zone. It should be noted that in 25–30% of rats, there are anatomical variations of coronary arteries of which the surgeon should be aware of in order to best manage cases and outcomes, but not all of these variations are considered anomalous [2, 11] (Fig. 2). The most common types of LAD arteries are those with 2–3 diagonal branches and a septal perforating branch. If the first diagonal is large, then the other diagonal vessels tend to be small and run shorter courses. Sometimes, it is possible to see right ventricular branches with the extension over the right ventricular surface (Fig. 2A, B, C). In some rats, there is a duplication of LAD (Fig. 2D) or early bifurcation of LAD (Fig. 2E). If a ramus intermediate artery is present, the diagonal vessels are less prominent and arise more distally (Fig. 2F).

Even the branching and position of the LAD artery is different in Sprague-Dawley outbred rats compared to Lewis inbred rats [21]. It is important that the investigator pays attention to the anatomy during the procedure to ensure the proper vessel is ligated and to avoid error and variability.

Ischemic heart failure

Despite significant progress in the prevention and treatment of cardiovascular diseases, the incidence and prevalence of HF have been steadily increasing in recent years. Currently, the leading cause of HF is ischemic heart disease which accounts for ~ 70% of HF incidence. Regardless of the etiology, ischemic HF is a complex disease of impaired LV function and structure [22]. Myocardial ischemia causes deterioration in LV function, which initially causes compensatory local and systemic changes in an attempt to maintain adequate stroke volume. These compensatory alterations included the Frank–Starling mechanism by an increase in preload, myocardial hypertrophy, activation of the sympathetic adrenergic, cytokine overexpression, and activation of the renin-angiotensin system. At the molecular level, HF is associated with abnormal excitation–contraction coupling, changes in extracellular matrix, shifts in gene expression, and programmed cell apoptosis. Finally, these events led to severe cardiac pump dysfunction, increased wall stress, and promote adverse pathological remodeling.

HF can be divided into two categories, i.e., HF with reduced ejection fraction (HFrEF) and HF with preserved ejection fraction (HFpEF) [23]. HFrEF is associated with systolic dysfunction and characterized by the inability of the heart to maintain cardiac output. In turn, HFpEF is associated with diastolic dysfunction while systolic function is normal. Interestingly, in the rat model of HFpEF, treadmill exercise intolerance developed earlier than hemodynamic abnormalities [23].

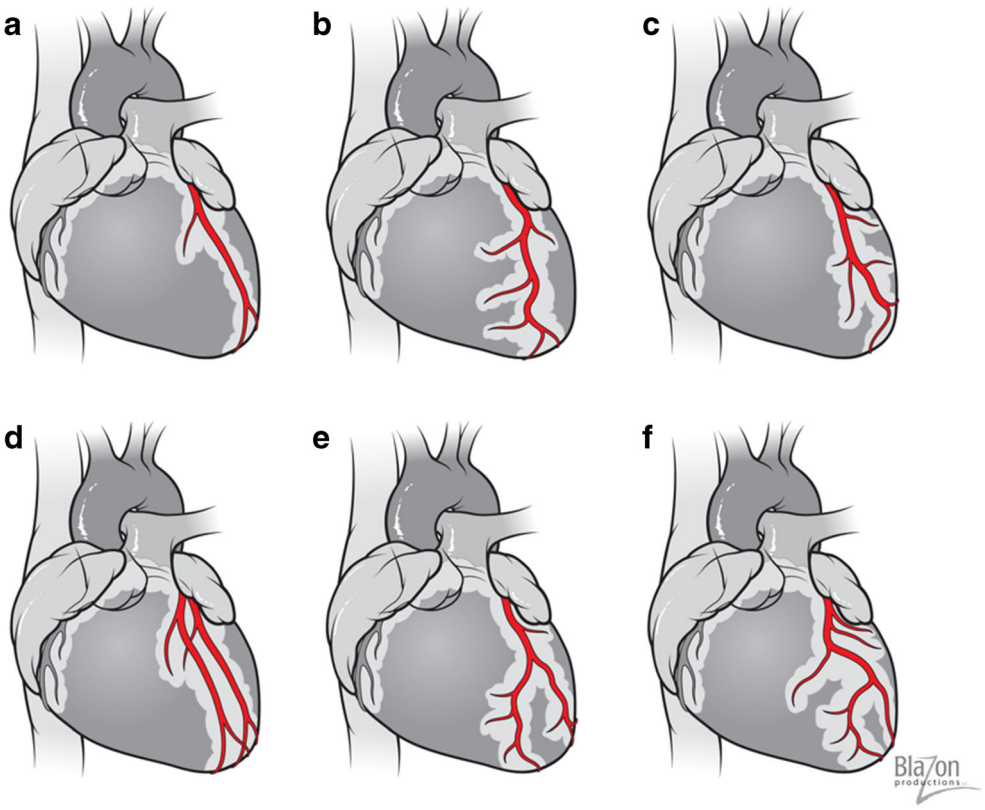

Fig. 2 Variability of rat's coronary arteries. (A, B, C) The most common types of LAD artery are with 2–3 diagonal branches and septal perforating branch. (D) Two left anterior descending arteries (duplication of LAD). (E, F) Left anterior descending artery has early bifurcation and does not reach the heart's apex. If a ramus intermediate artery is present, the diagonal vessels are less prominent and arise more distally

There are several reproducible animal models utilized to create ischemic HF. The classic model of myocardial infarction is created by complete ligation of the LAD artery. The ischemia/reperfusion model of ischemic HF is created by temporarily closing the LAD artery, then allowing blood to reperfuse through the LAD by releasing the closure.

Myocardial infarction

The permanent ligation of the LAD artery is a standard model for myocardial infarction followed by heart failure [17, 24].

Surgical technique

The animal's chest is prepped in sterile fashion by removing the hair on the chest and disinfecting the surgical area with three subsequent washes of 10% povidone-iodine, followed by 70% ethanol. Thirty minutes prior to surgery, all animals are injected with 0.1 mg/kg of the analgesic buprenorphine. For induction, the animal is placed into an appropriately scavenged inhalational isoflurane anesthetic chamber with 3–4% of isoflurane mixed with 100% oxygen flowing. After 3–5 min, the surgeon assesses the level of anesthetic depth by observing the loss of the righting and palpebral reflexes such as pedal reflex (firm toe pinch), and by muscular tone, response to painful stimulation, and the rate and depth of respiration. When the animal is fully sedated, an endotracheal intubation with a 16–18G catheter is performed. The anesthetized animal was placed in a right lateral semi-decubitus position on an isothermal heating pad to maintain body temperature around 37 °C. A rectal temperature probe is placed in the animal for temperature monitoring. The rat is connected to the ventilator and ventilated with 2–3% isoflurane mixed with 100% oxygen at the appropriate rate based on the animal's weight. The appropriate ventilation settings for rats are dependent on the animal weight and can be calculated according the following formulas: tidal volume (V_t, ml) = 6.2 $M^{1.01}$ (M = animal mass, kg); respiration rate (RR, min^{-1}) = 53.5 × $M^{-0.26}$. For example, in a 400-g rat, V_t = 2457 μl and RR is 68. Regularly monitor the depth of the anesthesia by checking the response to a tail pinch and make necessary adjustments of isoflurane if required to maintain the level of anesthesia [25].

Once the chest is entered via an 8–12-mm anterolateral thoracotomy incision in the 4th or 5th intercostal space, a chest retractor is placed, the lung is reflected posteriorly, and the pericardium is incised. The upper portion of the LAD is identified. This preparation is identical for all of the models of ischemic HF in this section. In this model, the LAD is completely ligated with a 7–0 prolene suture, with close attention being paid to electrocardiographic (ECG) abnormalities (Fig. 3a, b). Acute ST segment elevation, surrounding tissue discoloration distal to the suture, and dysfunction of the anterior wall confirm the complete surgical ligation of the LAD. Because of the intramural location of the LAD and anatomical variability, the surgeon sometimes needs to place additional sutures close to the pulmonary artery to get ECG changes specific for myocardial ischemia. Using ECG during the procedure provides a means to confirm successful MI creation regardless of anatomy [26]. Once hemostasis is achieved, a flexible chest tube catheter (16-G angio-catheter) is inserted through the 7th intercostal space under visual control. The ribs and intercostal muscles are closed with a 3–0 or 4–0 range prolene suture followed by closure of the chest using a 5–0 vicryl running suture. After tying these sutures, a 2–3-mL syringe is used to evacuate the air/fluid in the thoracic cavity in order to regain the normal negative pressure and then the chest tube is removed. The skin incision is closed using a running 5–0 vicryl absorbable suture. Following closure, isoflurane flow is halted and the animal is weaned from the ventilator. The animal is kept warm and allowed to breathe supplemental oxygen rate between 0.5–1 L/min via endotracheal tube. Following mobile signs of recovery, the animal is extubated. The animal should not be extubated before he is awake and breathing on his own. Supplemental oxygen may be given via nose cone or chamber if the animal still needs oxygen. The usual duration of the surgical part of procedure is about 15–30 min. The closure and recovery process must be completed for all procedures. The duration of recovery is unique to each animal.

Myocardial ischemia/reperfusion model

After an acute MI, the current most effective clinical strategy for reducing the MI size and improving outcome is myocardial reperfusion. Restoring coronary perfusion in a timely fashion can minimize the initial ischemia injury produced by occlusion of the LAD coronary artery. While this intervention has improved the number of survived animals after acute MI, restoration of blood flow into the ischemic area results in ischemia/reperfusion (I/R) injury that leads to the death of injured cardiomyocytes. This loss of myocardial mass contributes to decreased cardiac output and progression of HF. Thus, the study of the I/R injury is an important line of inquiry in cardiovascular research [27, 28].

Surgical technique

The LAD can be occluded two ways. The first technique is LAD occlusion with a suture above tubing. Once the location of LAD is confirmed, a 7–0 prolene ligature is passed underneath the LAD artery, a loose knot is made to leave a loop, and a 2–4-mm PE-10 tubing is placed inside the loop parallel to the LAD artery. The loop is tied around the artery and tubing (Fig. 4a). The chest retractor is removed, the lungs are re-inflated, and the wound is

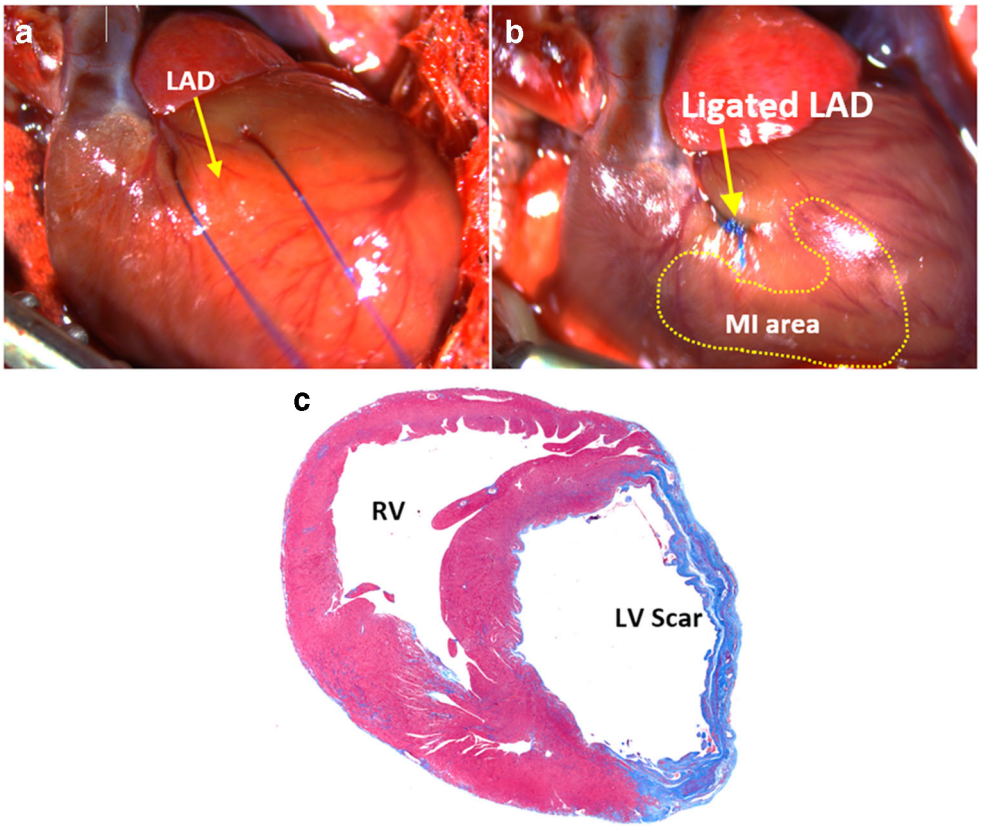

Fig. 3 Ligation the left anterior descending artery. **a** Prolene ligature is passed underneath the left anterior descending artery. **b** The left anterior descending artery is ligated with a prolene suture and myocardial infarction is created. The discoloration of the surrounding tissue and electrocardiography confirms the creation of an infarct. **c** Rat left ventricle was stained with Masson's trichrome and Weigert's iron hematoxylin. Blue area indicates left ventricular scar 4 weeks after myocardial infarction

temporarily closed with running 5–0 nylon sutures on the muscles and skin. The rat remains on the ventilator for the duration of the 30–60-min LAD artery occlusion, depending on the protocol. After this time has passed, the temporary sutures are removed, and the chest cavity is opened again. The ligating suture above the tubing is

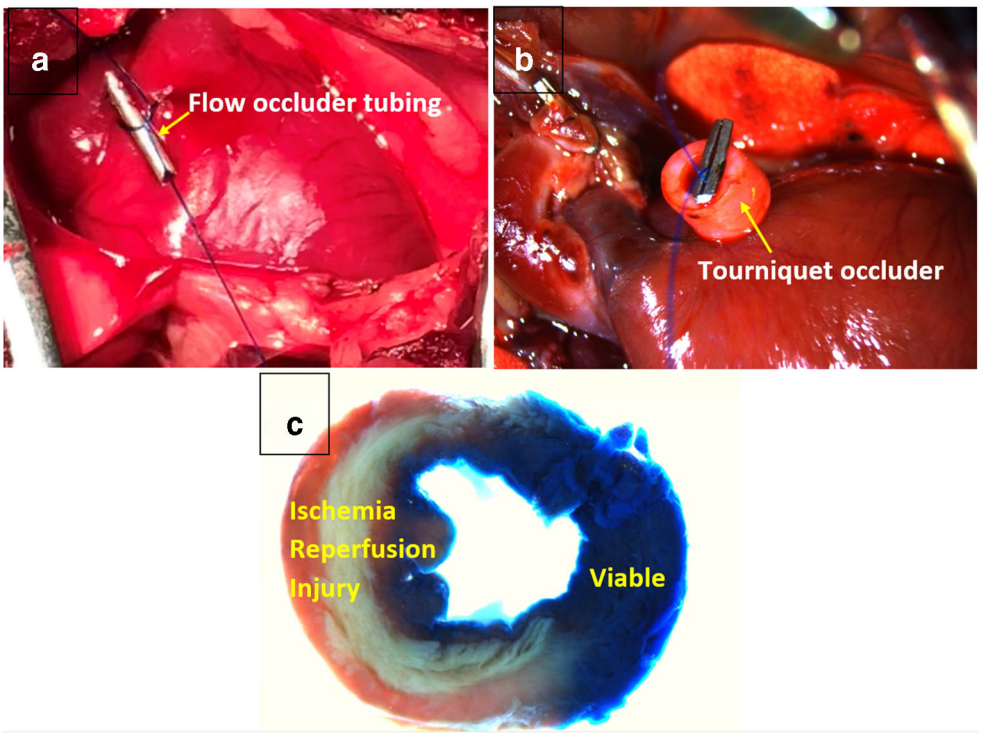

Fig. 4 Ischemia/reperfusion models. **a** Temporary occlusion of the left anterior descending artery with suture above the tubing. **b** Temporary occlusion of the left anterior descending artery with tourniquet. Ligature placed around the left anterior descending artery and secured by placing a tourniquet and clip to hold the suture in place. **c** Rat left ventricle was stained with triphenyltetrazolium chloride after induction of ischemia/reperfusion by temporary ligation of the left anterior descending artery. The unstained area is ischemic myocardium

cut and the PE-10 tubing is removed, allowing blood to flow back through the LAD artery.

In the second technique, the LAD is occluded with a tourniquet. Once the chest is open and retracted, a 6–0 or 7–0 prolene suture is placed through the myocardium and around the target site of the LAD artery. Both suture-free ends of the ligature are passed through the small tourniquet (PE rubber tube) (Fig. 4b). The snare loop is tied and the myocardium visually inspected for a short period of time. The temporary snared occlusion of the LAD artery should produce cyanosis of the anterior and lateral walls of the left ventricle and changes in ECG readings. The chest is temporarily closed for 30–60 min, depending on the protocol. The tourniquet is removed, allowing blood to flow through the LAD. Reperfusion can be verified by the return of the red color to the myocardial tissue and the demonstration of some recovery of the anterior wall motion [29]. The animal's chest is then closed and the animal moves to recovery, same as in the myocardial infarction model.

Challenges in creating ischemic heart failure

There are several considerations that need to be addressed to facilitate creating ischemic HF. There is no standard definition of HF in rodents currently accepted by investigators [30, 31]. Thus, it is important to define what symptoms and which type/severity of HF is being studied in order to establish a timeline for the study. Acute MI in rodents causes ischemic HFrEF [22]. The clinical signs such as lack of movement, decrease of the body temperature and weight, tachypnea, and labored respiration are very helpful to assess development of HF. Other clinical features such as pleural effusion, ascites, and pulmonary and hepatic congestion can be analyzed as well [32]. Also, HF biomarkers, like natriuretic peptides, cardiac tropins, and growth differentiation factors, offer biologically relevant insight on HF progression [33]. An important aspect for defining study timelines is measuring heart function. Most researchers prefer to use cardiac imaging technology such as echocardiography, magnetic resonance imaging (MRI), and computer tomography to measure regional and global heart function and assess HF development [34–36]. More sophisticated methods include positron emission tomography and nuclear magnetic resonance spectroscopy [37].

There are several HF timelines described in literature. Many authors believe that the HF changes with cardiac remodeling and infarct expansion are more pronounced at 21–28 days after MI creation [38–40]. Some authors found that after 7 days, rats with large MI have decreased contractility, which does not change significantly at 30 days [41]. Other authors demonstrated increased LV dimensions in systole and diastole after 7 days, and even after 5 weeks, these parameters did not change significantly [42]. In other studies, LV systolic and diastolic dysfunction was apparent 8 weeks after MI creation [43–45]. On average, clinical signs of HF develop after 3–6 weeks. In cases of larger infarct, the ventricle becomes distended and dilated faster [24, 46–50]. The discrepancy in HF progression in infarcted rat hearts with a wide range of LV dilatation and contractile dysfunction at different time points probably connected to the variability in LV remodeling and MI expansion after LAD ligation.

The third consideration is the infarct size created. In fact, the degree of LV remodeling and chamber dilatation is directly proportional to the infarct size [51]. Moreover, the rat's survival is directly related to the size of myocardial infarction. In small MI (< 20%), the survival rate at 60 days was ~ 85%, and in large MI (> 45%) was ~ 60% [41, 42, 52–54]. Therefore, it is necessary to demonstrate equivalence of infarct size between animal groups when comparing subsequent remodeling responses [2, 30]. The minimum infarct size to cause these morphological, functional, and clinical abnormalities of severe HF is 36–40% [55]. However, an infarct size of 23% of LV is characterized by a 27% increase in volume of the remaining functioning myocardium [52]. Infarct size varies depending on the anatomical variability of the pattern of coronary arteries, place of LAD artery occlusion (proximal, middle, or terminal), extension of ischemia, and the collateral flow to that area [24, 56]. For most studies, the LAD artery is ligated at the proximal part 1–2 mm below the tip of the left atrial appendage which induces infarction, forms a scar on roughly 40–55% of the LV, and creates severe HF (Fig. 3c) [24, 46, 47, 50, 57]. However, LAD artery occlusion in this location suffers from the drawback of a high mortality rate [24]. LAD ligation in the middle part 3–4 mm below the junction of pulmonary conus and left arterial appendage induces infarction, scars 30–35% of the LV with low mortality (10–25%), and creates moderate HF [58, 59]. Development of severe HF with this ligation takes longer. In small and moderate MI size (15–35%), 80–90% of rats survive to 60 days. In large MI (MI size > 45%), only 40–60% of rats survive to 60 days [41, 42, 52–54].

The effect of I/R on cardiac remodeling depends on duration of cardiac ischemia, reperfusion time, and size area of myocardial risk. Reperfusion after 45 and 90 min resulted in an infarct size of 36% and 38% respectively. Late reperfusion after 180 min resulted in an infarct size of 49% [57]. In another study, 45 min of ischemia followed by reperfusion resulted in an infarct size of only 22% but an area of risk of 48% [60]. Reperfusion after 120 min of coronary occlusion increased the area of risk to more than 50% [61]. To assess the area of ischemia during rat's euthanasia, a loose suture knot should be retied during heart perfusion with ink to delineate the area of risk of I/R (Fig. 4c).

One of the frequent complications after creation of ischemic HF in rats is cardiac arrhythmia, accompanied by significant mortality [62]. Post-MI arrhythmia usually occurs in the

early period after MI. Ninety-six percent of animals developed at least one episode of ventricular tachycardia (VT) or ventricular fibrillation (VF) during the first 48 h after occlusion LAD with different MI sizes ranging from 23 to 67% [57]. Antiarrhythmic drugs and regimes may be given at different time points before and during the procedure [63–66]. To prevent arrhythmias, pretreatment 10–15 min before coronary occlusion with intravenous administration of class I antiarrhythmic agents like lidocaine (2 mg/kg), procainamide (20 mg/kg), or quinidine (10 mg/kg) produced significant reductions in the number of rats demonstrating VF [67–69]. Good antiarrhythmic efficacy was reported after intravenous injection of amiodarone (class III agents) (100 mg/kg) 5 min post-MI creation and after chronic oral amiodarone administration (30 mg/kg) for 2 weeks. Compared with controls, both treatment regimens decreased the number of VT/VF episodes by ~ 85% [70, 71]. In a rat study treated with calcium antagonists (class IV agents), diltiazem (2.0 mg/kg), verapamil (5 mg/kg), or nifedipine (50 μg/kg) was given as an intravenous bolus 10 min prior to coronary occlusion. All three calcium antagonists significantly reduced the incidence of VF and this anti-fibrillatory effect resulted in a significantly lower mortality in all drug-treated groups. With diltiazem, verapamil, and nifedipine, mortality fell from 87 to 35%, 0%, and 8% respectively [72–74].

Finally, there are important technical challenges that need to be addressed. In some cases, LV recoloration, indicating reperfusion, does not return after releasing the LAD snare. In this case, it should be considered that the artery was damaged with a needle or clot and these animals have to be excluded from the study. To prevent myocardial damage or transection of the artery by the ligature, the suture should be placed slightly deeper in the myocardium. It is better to use sutures with Teflon pledgets as buttresses under the knot to prevent LAD rupture.

For all models of ischemic HF, it is essential to monitor body temperature especially for the I/R model because it is a longer procedure. A drop in temperature can alter the rat's heart function and body metabolic reaction with energy homeostasis, and can affect the size of myocardial ischemia [32]. In order to increase survival and efficacy in this model, investigators must temporarily close the chest prior to the reperfusion [75, 76].

One of the major issues of creating ischemic HF in rats today is mortality. Mortality after MI creation in the rats should be divided into early and late HF-related death and non-HF death. The usual causes of early non-HF mortality are poor surgical technique, non-observance of acceptable guidelines of rodent's intubation, ventilator weaning and post-operative care, non-use of physiological systems for monitoring SpO_2, exhaled CO_2, ECG, and rectal temperature. It is interesting to note that after MI creation, the overall mortality rate and post-MI recovery time between younger and older rats are different [41]. The use of younger animals (4–6 weeks old, 200–350 g) may reduce non-HF mortality.

Left ventricle pressure overload models

Aortic banding

Aortic banding is a classic model of HF and is used to induce left ventricular overload. Aortic banding techniques are applied to achieve aortic stenosis via the ascending aortic constriction (AAC), transverse aortic constriction (TAC), or abdominal aortic constriction. The difference between these models is the location of the surgically applied constrictor. In the AAC model, the constriction is made in the ascending aorta before brachiocephalic trunk, decreasing blood flow to both left and right carotid arteries. This leads to the fast development of high pressure in the LV and corresponding rapid changes in LV anatomy and function [77–79]. In the TAC model, stenosis is typically created in the aortic arch between the brachiocephalic trunk and the left carotid artery. With this technique, only the left carotid artery has diminished blood flow and the right carotid artery remains open to blood flow. The pressure in the LV cavity and LV hypertrophy in TAC model rises more gradually than in AAC model [80]. In abdominal aortic constriction, stenosis is located below renal arteries; therefore, the brain's and other major organs' flow reserve is not changed. Some researchers use aortic banding above the renal arteries as it creates a model where elevation of the blood pressure is generated by mechanical obstruction and activation of the renin-angiotensin-aldosterone system due to reduced renal blood flow [23].

Surgical technique

While there are a variety of surgical approaches that are established to create aortic stenosis, most studies use the right thoracotomy. The animals are intubated and placed in a right or left decubitus position, and the chest is prepped in sterile fashion as described in the section "Myocardial infarction, surgical technique." The thoracotomy is performed, with an 8–12-mm incision in the second intercostal space. The lung is moved out of the way using a small piece of gauze or cotton-tipped applicator to avoid injury. The thymus is retracted to view the underlying structures.

The aorta can be ligated one of three ways: using ligature with needle retraction, hemoclips, or a tourniquet.

Banding of ascending aorta

The usual diameter of the aorta in 250–450-g rats is 2–3 mm. After blunt dissection of the aorta, a 4–0 silk is advanced underneath the aorta, ligating in the location according to the

AAC or TAC model, and a loose knot is tied. A needle is advanced alongside the vessel, through the loose knot. Aortic constriction is achieved by ligating the silk ligature around the vessel and the needle, creating occlusion [81, 82] (Fig. 5a). The needle is then immediately removed, leaving a lumen with a severely stenotic aortic orifice. After completing banding, a trans-thoracic Doppler echocardiography is performed to determine the intensity of the pressure overload produced by the constriction. The thoracotomy is then closed and air is evacuated from the chest. Recovery from anesthesia commences with the animal being weaned from the ventilator.

The aorta can be banded using clips via surgical applicator [79, 83–86]. In this approach, a tantalum clip is placed around the aorta rather than a suture. The clip is precisely half-closed around the aorta by means of a clip applicator with an adjustable clamp (WECK, Horizon, Metal Ligation System, Morrisville, NC, USA). The blood flow through the aorta is restricted to the diameter of the inner segment of the half-closed clip. This approach achieves the same result as the previous aortic banding methods but the device is more consistent and the degree of stenosis is more controlled. It is necessary to consider the diameter of the ascending aorta, which is dependent on rat weight [78].

The tourniquet technique can also be used. To band the aorta, a suture is passed underneath the aorta and the two ends of the suture are threaded through a 0.5-mm piece of polyethylene (PE-10) tubing (Fig. 5b). When the tourniquet is partially closed, the stenosis is created. This procedure is better to perform under the control of Doppler echocardiography to confirm the degree of stenosis.

Banding of abdominal aorta

The surgical technique is somewhat different when performing the abdominal aortic banding technique. Once the animal is prepared for surgery, he is placed on his back. The chest is prepped and a midline abdominal incision is made. A retractor is inserted and all of the large and small bowels are pulled out of the abdominal cavity and kept wrapped in gauze soaked with sterile saline to the left of the opening. The rat's retro-peritoneum is blunt dissected to get a clear view of the aorta. The abdominal aorta is isolated adjacent to renal arteries, and constricted by a 4–0 silk suture ligature tied firmly against a 21- or 22-gauge needle. The needle is removed immediately and the aorta remains constricted to 0.5–0.7 mm in diameter [87, 88]. The bowel is returned to the original position and the abdomen is closed with a 5–0 vicryl suture. The tourniquet and clip method can also be used.

Right ventricle pressure overload models

Pulmonary artery banding

Overall, the techniques used to create right ventricle pressure overload with pulmonary artery (PA) banding are the same as aortic banding. The initial steps to prepare and open the animal are similar to those in the previous section. The thoracotomy is performed in the 2nd–3rd intercostal space and the PA is visualized.

The site of band placement is the middle portion of the PA trunk. The PA should be handled carefully because it is thin-walled and susceptible to injury. To minimize injury, the ligature must be first passed through the transverse sinus to encircle the aorta and PA. Then, the aortic end of the ligature is passed between the aorta and PA so that only the PA is enclosed in the ligature. To band the PA, investigators may use a tourniquet, in which the band is snared with a short segment of polyethylene tubing and secured with small hemoclips. Many researchers utilize PA ligation with needle retraction. A silk suture is tied tightly around an 18–21-G needle alongside the main PA. After subsequent rapid removal of the needle, a fixed, constricted lumen remains equal to the diameter of the needle [89–93]. The combination of fixed banding around the pulmonary artery and natural growth results in a progressive increase in right ventricle (RV) pressure and pressure gradient and RV hypertrophy, usually after 6–8 weeks [94, 95]. The clip technique involves placing a clip around the PA and closing it partially, so that only ~ 50% of

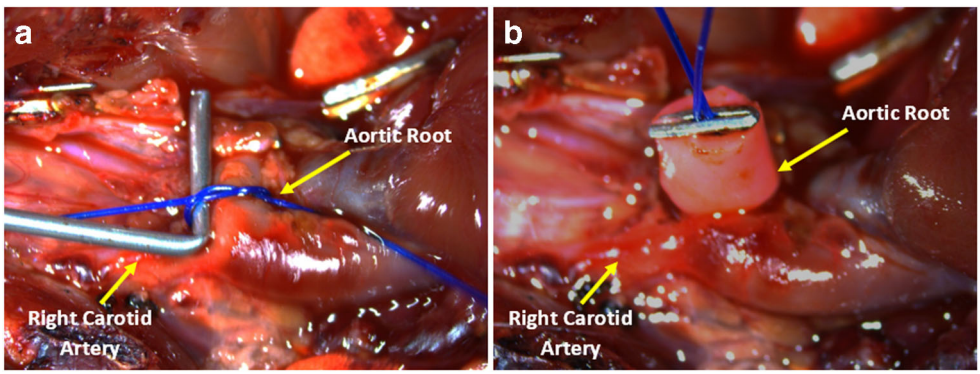

Fig. 5 Aortic banding techniques. **a** Aortic banding using ligature and needle retraction. Ligature is tied around the aortic arch and needle. Afterwards, needle is removed to allow reduced flow. **b** Aortic banding using a tourniquet technique. Ligature placed around the aorta and secured by placing a tourniquet and clip to hold the suture in place

the lumen is opened. In order to place the clip, the surgeon has to place a ligature first around the PA so as to fully access the vessel [89, 92]. This technique is gaining popularity because it is simple and yields more consistent results.

Challenges in creating pressure overload models

There are several challenges that need to be addressed to facilitate a successful aortic banding. The timeline for creating HF by pressure overload is longer compared to ischemic HF models. In response to the development of chronic pressure overload, ventricular wall thickness increases to maintain normal wall stress. This compensatory mechanism is accompanied by concentric myocardial hypertrophy [96]. Over time, the compliance of the ventricle is reduced, which impairs flow filling and leads to diastolic dysfunction. Eventually, the diameter of the ventricle increases, concentric hypertrophy shifts to eccentric with both systolic and diastolic dysfunction, and signs of HF appear [30, 97]. After ascending aortic constriction, left ventricular hypertrophy develops at 6–8 weeks and clinical signs of HF appear within 20–30 weeks [78, 83, 86, 98]. It was demonstrated that the transition from concentric hypertrophy to eccentric hypertrophy with HF after aortic constriction occurs after 20 weeks [99].

The next important consideration is the degree to which the aorta must be constricted to produce myocardial hypertrophy. Many researchers use a vascular clip with a small internal diameter 0.6–1.0 mm to constrict the aortic diameter by ~ 50% [83, 98]. Others use vascular clips with large diameter of ~ 1.5 mm to create aortic banding [100, 101]. Stenosis of the ascending aorta to 50% of its original diameter leads to the appearance of a pressure gradient of at least 50–60 mm of Hg at the aortic constriction site [102]. Some researchers believe that for faster development of a concentric hypertrophy (within 6 weeks), the aortic pressure gradient has to be about 90 mmHg [82, 103].

Abdominal aortic banding is more advantageous than the AAC and TAC models. There is no need to intubate the animal during the procedure and post-operative recovery is much easier. Furthermore, this procedure does not disrupt blood flow to the brain, unlike the AAC and TAC models. However, in this model, hypertrophy and HF develop much slower [88, 104].

High-resolution echocardiography has become the non-invasive method of choice for determining myocardial hypertrophy, assessing systolic and diastolic function, and classifying HF stages in pressure overload models. In order to fully assess HF, several principles of echocardiography are used [79, 80, 101, 105–108]. Parasternal long and short axes—at the level of papillary muscle—are obtained to calculate the LV end-diastolic and end-systolic volumes as well as the ejection fraction of the LV using the area length method: $V = 5/6 \times A \times L$, where V is the volume in milliliter; A is the cross-sectional area of the LV cavity in square centimeters, obtained from the short-axis image in diastole and in systole; and L is the diastolic length of the LV cavity in centimeters, measured from the long-axis image as the distance from the endocardial LV apex to the mitral-aortic junction. 2-D-guided M-mode images are obtained from the short-axis view of the LV at the level of the papillary muscle to measure the thickness of the septum and the posterior wall at the end-diastole as well as the LV end-diastolic and LV end-systolic internal dimensions and to calculate LV fractional shortening. Pulsed Doppler signals of the left ventricular inflow should be assessed in the apical four-chamber view. To measure cardiac output, the Doppler can be placed in the apical long-axis view. Diastolic function is usually evaluated using pulsed Doppler to assess mitral valve velocity during the fraction of the cardiac cycle. To image the constricted aorta, a Doppler probe is placed on the left and right carotid arteries to determine the intensity of Doppler velocity signals. Moderate degrees of constriction create a right carotid/left carotid ratio of 5–8 and a severe form leads to a ratio of 8–10.

There is a great interest in MRI as a non-invasive cardiac imaging modality that can provide precise ventricular morphology with high spatial and temporal resolution and good soft-tissue contrast without radiation in the rat models of HF. The MRI assessment of myocardial extracellular space using kinetics of contrast agent (gadolinium) has been introduced as a marker of myocardial necrosis in ischemic heart disease. Being non-invasive and exact, MRI can offer new insights of rat cardiac morphology and function and can shed new light on the pathophysiology of cardiac remodeling and ongoing changes of the post-MI scar [109, 110].

An invasive catheterization pressure measurement with pressure-volume methodology probably is the best and a very accurate tool for confirming hemodynamic changes in rats with aortic banding. The advantage of this method is that it enables to characterize the LV performance independently from loading conditions and heart rate. Thanks to advances in microsensor technology, this approach has been successfully translated to rat models [25].

However, this method is invasive and used before euthanasia or sometimes during surgery immediately after creating aortic constriction [79, 100, 111]. In the TAC model, two catheters connected to a high fidelity pressure transducer (Millar Instruments, Houston, TX, USA) should be placed in the right carotid (proximal pressure) and femoral artery (distal pressure) and the gradient between them will demonstrate the level of aortic stenosis (Fig. 6a). In the AAC technique, a left ventricular puncture is required through the heart apex for the measurement of the proximal pressure and the second catheter (distal pressure) should be in the femoral or carotid artery (Fig. 6b). Undoubtedly, the pressure gradient is very important to

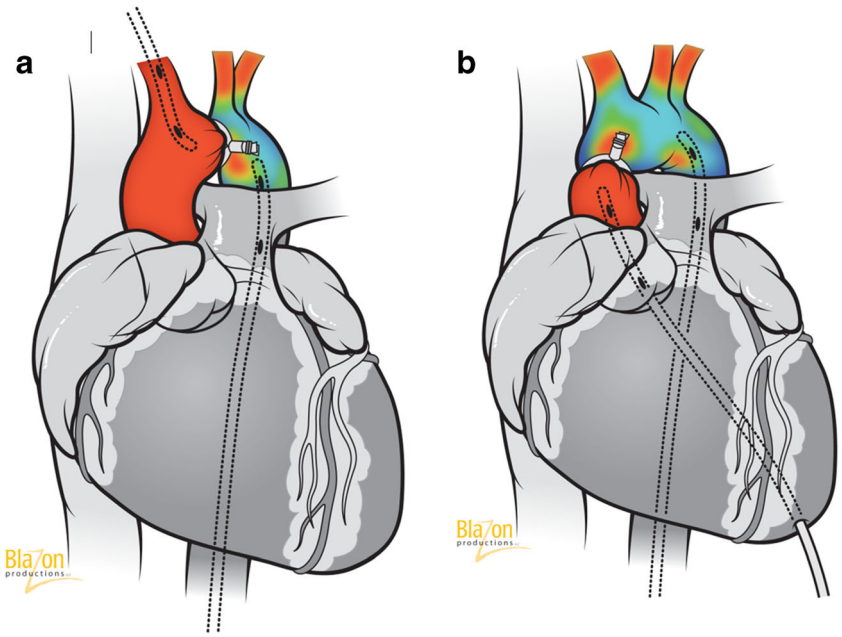

Fig. 6 An invasive catheterization technique to measure pressure gradient in rats with aortic banding. **a** Catheterization technique in transverse aortic constriction model. Two catheters connected to a pressure transducer should be placed in the right carotid and femoral artery. Pressure gradient between them demonstrates the level of aortic stenosis. **b** Catheterization technique in ascending aortic constriction model. Two catheters connected to a pressure transducer should be placed in the left ventricle and in the femoral or carotid artery. Pressure gradient between them demonstrates the level of aortic stenosis

measure degree of aortic stenosis. However, it should be noted that in the TAC model, the gradient increases gradually for a few weeks before it stabilizes and then declines as cardiac failure develops. In summary, the advantage of the TAC model and abdominal banding is a very low overall mortality rate since the onset of disease is progressive. However, high survival rates render this model poor since subsets of animals do not develop signs of severe cardiac hypertrophy and HF. In the AAC model, severe hypertrophy develops faster but the survival rates are lower.

In 15–20% of cases, aortic banding is complicated by band internalization (erosion) through the aortic wall. This results in an increased cross-sectional area and reduced LV pressure afterload with no development HF [112]. The reason band internalization occurs is probably connected to the surgical technique suture material used. Using polypropylene sutures can induce an inflammatory and immunologic response with band internalization [113]. Thus, it is probably better to use silk sutures instead of polypropylene.

Under normal physiological conditions, the pulmonary circulation is a low-pressure system, with low vascular resistance. When RV afterload increases progressively, significant RV adaptation occurs to sustain a near-normal cardiac output for prolonged periods of time [94]. Three weeks after PA banding with a clip with an outer diameter of 1.7 mm (moderate stenosis), there was an increase in RV index by 72%, RV systolic pressure by 84%, and RV end-diastolic pressure from 3.6 to 5.4 mmHg [89]. Whereas the initial PA banding in rats weighing ~ 200 g was mild, the combination of a fixed PA constriction and animal growth resulted in a progressive increase in RV systolic pressure and a pressure gradient of ~ 50 mmHg after 6 weeks. An increase in mortality and HF did not develop until 22 weeks after the procedure [94]. Mild to moderate PA banding resulted in an increased RV pressure by ~ 60% and a twofold increase in RV mass after 6 weeks, with only compensatory RV hypertrophy [90]. More severe constriction tripled the RV index, resulting in severe diastolic dysfunction with increased end-diastolic pressure (EDP) from 2.4 to 10.3 mmHg after 4 weeks and finally RV dysfunction with HF [93]. Remarkably, when comparing PA ligation with needle removal and ligation with clips, surgical mortality was significantly lower in the needle removal group (3.6% versus 25%) while echocardiography revealed more severe signs of RV decompensation like pleural and pericardial effusion in the clip technique group [92].

Heart failure due to volume overload models

The cardiovascular remodeling secondary to chronic volume overload is characterized by progressive ventricular dilatation, hypertrophy, and ultimately HF [114]. Ventricular dilatation without appropriate hypertrophy in volume overload models can induce myocardial dysfunction and is therefore responsible for the faster development of HF [115]. Several experimental models of volume overload are available for the creation of HF in the rats [30]. The most popular models of volume overload in rats are the generation of abdominal aorta-vena (AV) cava fistula (aorto-caval shunt) and aortic valve regurgitation [116–125]. Hemodynamic data in these models suggest a sustained elevation of LV diastolic volume. The maintenance of high-output status at early stages after creation of AV shunt relies on the Frank–Starling mechanism. This change reflects the sudden increase of wall stress due to the

volume overload, whereas the changes in LV end-diastolic pressure indicate that the developing of the cardiac hypertrophy and dilation of the cardiac chamber tend to normalize the wall stress. There is a strong correlation between increased end-diastolic loading of the LV and myocardial remodeling, which eventually results in marked ventricular dilatation and decreased ventricular stiffness and contractility. Further deterioration of the diastolic function is consistent with development of HF.

Aorta-venous shunt

Surgical technique

A midline abdominal incision is made from the xyphoid to the pubis. A retractor is inserted and all of the large and small bowels are pulled out of the abdominal cavity and kept wrapped in gauze soaked with sterile saline to the left of the opening. The rat's retro-peritoneum is dissected to get full view of the aorta and the inferior vena cava (IVC). The infra-renal portions of the aorta and IVC are exposed at the site where the two vessels share a common fascia (Fig. 7a). At this site, a 7–0 prolene purse suture is applied on the top of the anterior wall of the aorta. The supra-renal portion of the abdominal aorta is then occluded with a microsurgery clip to control for bleeding. The side-to-side shunt is then created with the use of an 18-gauge angio-catheter inserted through the purse suture on anterior wall of aorta, puncturing the posterior aortic wall, and advancing the needle into the IVC. The needle is pulled back a little bit and only the catheter is advanced into IVC (Fig. 7b). Then, the angio-catheter is withdrawn, the purse suture is tightened, and the clip occluding the aorta is released. After de-clamping the aorta, arterial blood mixes with venous blood in the IVC, which causes distension and pulsation of the IVC. Routine

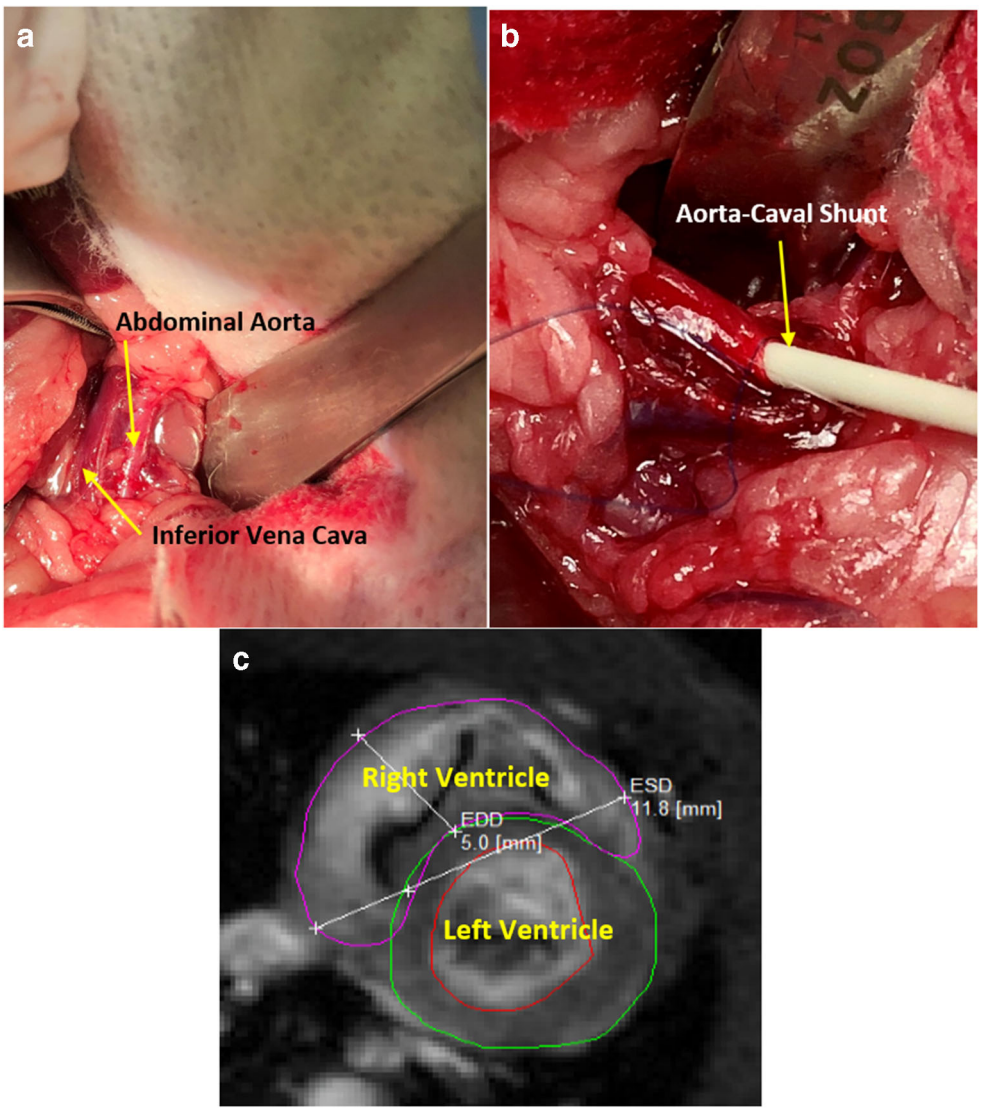

Fig. 7 **a** Surgical exposure of the rat's abdominal aorta and inferior vena cava. **b** Aorta-caval shunt creation featuring the advancement of angio-catheter. **c** MRI of the left and right ventricles in the short-axis plane following aorta-caval shunt creation. Ventricle dilatation in dimensions is shown in the end-diastolic phase

palpation in the anastomotic region helps to feel the pulsation as a sign of AV shunt patency. The bowel is returned to the natural position and the abdomen is closed with a 5–0 vicryl suture.

Aortic regurgitation

Severe aortic regurgitation (AR) imposes another volume overload model of HF. The volume overload is a consequence of the regurgitating ventricular volume itself and is therefore directly related to the severity of the aortic insufficiency. Whereas mild AR produces only minimal volume overload, severe AR can produce massive LV volume overload and progressive chamber dilatation. AR can be categorized as compensated or decompensated. In compensated AR, the LV initially adapts to the volume overload by eccentric hypertrophy, which preserves LV diastolic compliance, such that LV filling pressures remain normal or mildly increased despite a large regurgitate volume. In decompensated AR, LV systolic dysfunction is accompanied by decreased LV diastolic compliance as a result of hypertrophy and fibrosis, leading to high filling pressures and heart failure symptoms.

[114].

Surgical technique

Experimental AR in rats can be induced by perforation of the aortic leaflets with a wire by mechanical interruption. The animal is placed in the supine position under anesthesia with mask isoflurane 3–4% and 100% oxygen. A right or left lateral neck incision is used to expose the common carotid artery. Ligature is placed under the carotid artery for control and the distal part of carotid artery is ligated with a 4–0 prolene suture. An arteriotomy between the proximal and distal parts is then performed to allow the insertion of a 0.9-mm guide wire or long angio-catheter 22–24 G or epidural catheter 20 G. The echocardiographic probe is positioned on the thorax to obtain a view of the left ventricle, the aortic valve, and the ascending aorta equivalent to a parasternal long-axis view in standard echocardiography study. Under echocardiographic guidance, the angio-catheter or guide wire is advanced towards the aortic valve in a retrograde manner until resistance from one cusp of the aortic valve is felt. The wire is then advanced a few millimeters to perforate a cusp of the aortic valve. The resulting tear in the leaflets induces an acute AR. Aortic insufficiency is considered moderate to severe in the instant following echocardiographic criteria at the time of surgery; color Doppler ratio of the regurgitation jet width to LVOT diameter was 50–70%, and pulsed-wave Doppler confirming reversed diastolic flow in the abdominal aorta. Leaflet perforation can be repeated when the severity of the regurgitation jet in the abdominal aorta is considered insufficient by echocardiographic criteria. When the generation of AR is completed, the proximal carotid artery is ligated with 4–0 prolene sutures and the neck wound is closed with a 5–0 absorbable suture.

Another surgical approach is through a left thoracotomy in the fifth intercostal space after endotracheal intubation with isoflurane 2–3%. The LV apex is exposed and a 7–0 prolene suture with tourniquet is placed there. The angio-catheter 20 G is inserted through the suture and a guide wire is inserted into the LV via angio-catheter. The wire is moved up to the aortic valve where leaflet perforation occurs guided by intra-cardiac echocardiography. The 7–0 prolene suture is tied to close the hole in the LV and the chest is closed with a 5–0 absorbable suture.

Creation of AR causes immediate changes in LV end-diastolic pressure from 4.8 to 12 mmHg [126, 127]. The resulting tear in the aortic leaflets induces an acute AR. A 30% decrease in aortic diastolic pressure is considered a sign of severe AR [116, 120, 122, 128].

Challenges in creating volume overload models

The relationship between heart weight and body weight is one of the most used analytical endpoints in the study of HF in the rats. A higher ratio is a sign of HF progression [129]. The creation of the AV shunt increased total heart weight-to-body ratio of 45% and RV weight-to-body ratio of 65% after 5 days, compared to control animals [124]. This ratio is time-related and continues to increase with time. It was shown changes in this ratio from 78% at 4 weeks to 87% at 10 weeks after AV shunt creation [121]. By 8–10 weeks, sustained RV overload leads to progressive ventricular dilatation with heart decompensation [115, 117]. This endpoint can be useful when dealing with compensatory hypertrophy, where the body weight theoretically remains stable but the heart weight increases. However, the body weight of the rat is not stable. As the rat develops HF, the body weight changes due to growth; the enlargement of other organs, such as the liver and spleen; and pleural and abdominal exudate. Thus, this endpoint may not be an accurate way to assess HF development.

The size of the AV shunt plays a role in the timeline of HF development. It was demonstrated that after 8 weeks, bigger shunt size is linked to a significant increase in RV, lung, and liver weight. Cardiac dilatation assessed by LV end-diastolic diameter was 1.4 times greater in the large AV shunt group than in the small AV shunt group. Moreover, postmortem examination visualized clear signs of HF including dilated heart, congested liver and lung, and presence of ascites and pleural effusion more consistently in the large-size-shunt group [125, 130–133]. Interestingly, the size of the AV shunt can change in the post-surgical period. It was demonstrated that AV shunt with a diameter 0.17 mm at 1-day time point

increased to 0.35 mm at 2 weeks and after that was stable. Similarly, the flow velocity calculated by Doppler significantly increased from a baseline velocity of 18 cm/s to 34 cm/s after 2 weeks [134]. After 2 weeks, the diameter and velocity stabilized. Therefore, the patency and the size of the shunt should be measured at different time points.

To confirm the shunt patency, it is useful to use visual distension and pulsation of the IVC during the procedure and routine palpation of the abdomen to feel the thrill [121]. Oxygen saturation measurement is a very accurate tool that can verify arterial-venous blood mixing in the post-surgical period. In blood samples of rats with an AV shunt, oxygen saturation in the IVC above the shunt was markedly higher [121]. Doppler ultrasound should be performed to confirm the presence of the AV shunt and measure the flow through the shunt. For these purposes, authors use high-resolution imaging system with a probe frequency of 20–60 MHz [132]. For confirmation of an AV shunt, the waveform in the inferior vena cava was recorded using pulse-wave mode. The presence of arterial or turbulent waveforms in the IVC was regarded as a patent AV shunt. Flow velocity can be measured by ultrasound and sheer stress can be calculated using the Hagen-Poiseuille equation [135]. The patency and flow rate of the AV shunt can be also evaluated using ultrasound biomicroscopy with a Transonic flow meter [136] and radioactive microspheres [137]. Finally, MRI is also very useful and can show progressive dilative hypertrophy of the right ventricle (Fig. 7c).

The calculation of AV shunt potency is an important measurement in order to ensure that volume is enough to create HF but not so large that the animal will die. In the intact circulation without an extra- or intra-cardiac shunt, the total amount of blood ejected from the pulmonary artery is equal to that ejected from the ascending aorta [114]. The pulmonary blood flow (Qp) is, therefore, equal to the systemic blood flow (Qs) and the ratio of these two circuits (Qp/Qs) is equal to one. In AV shunt, the blood from one arterial circuit passes to the venous circuit. Therefore, the ratio of Qp/Qs becomes greater than one. The calculation of the magnitude of the shunt requires the measurement of oxygen saturations in the systemic and pulmonary circulations and can be determined by formula $Qp/Qs = (SAO_2 - MVO_2)/(PVO_2 - PAO_2)$, where SAO_2 is the arterial oxygen saturation, MVO_2 is the mixed venous oxygen saturation, PVO_2 is the pulmonary venous oxygen saturation, and PAO_2 is the pulmonary arterial oxygen saturation [138]. It was demonstrated that 10 weeks after AV shunt creation, Qp/Qs was 2.12 compared to 1.0 in the control group ($p < 0.05$) [139]. If the ratio is approximately 2, HF will develop in 8–12 weeks. If the ratio is more than 3, HF will progress very quickly.

The side-to-side infra-renal aorta-caval shunt created with use of an 18-gauge angio-catheter is the most popular AV shunt technique used by many researchers. Techniques with arteriotomia and venotomia and vascular side-to-side aorto-caval anastomosis are far less popular due to the surgical complications and difficulties of achieving a good shunt size [137]. The femoral artery to femoral vein shunt is another AV shunt that is used to create volume overload [118]. The main limitations of this technique are that the femoral vessels are smaller and the surgeon needs to ligate of the distal part of the common femoral artery, so the animal will also have an ischemia of the leg. Interestingly, comparing femoral and aorta-caval shunt, it was found that after 10 weeks, ratio of heart weight/body weight of rats increased only on 15% with femoral fistulas and 41% with aorta-caval fistulas compared to baseline [118]. Some investigators create volume overload by using another technique which involves placing a venous graft between the abdominal aorta and inferior vena cava, performing an anastomosis of renal vessels to the abdominal aorta, or performing an anastomosis between the iliac-lumbar vein and aorta [131, 136]. Some researchers seal the aortic puncture site with biological glue (cyanoacrylate) instead of tying a purse suture. The limitations of this technique include failure of sealing with bleeding from the puncture site, spreading of the glue to the neighboring tissues resulting in tissue hardening, poor visualization of the shunt, and extravasation of glue into the vessel with shunt occlusion [125, 140]. Other technical complications of this model include occlusion of the flow in the distal part of descending aorta, vena cava thrombosis, bleeding, and shunt stenosis [121, 124, 133, 134].

There are several challenges regarding the creation of aortic regurgitation. One of the major problems is the rather high mortality rate due to cardiac failure associated with the acute AR. Creation of multiple aortic valve leaflet perforations lead to severe valve destruction, intractable HF, and death. Thus, wire perforations should be performed under echocardiography control and multiple perforations should be avoided [120]. Another challenge is the size of the wire for perforations. Some researchers prefer bigger wires (0 .9mm), which can cause multiple leaflets injury with severe AR, while others prefer smaller wires (0.3 mm), which produces very mild AR [120, 122, 127, 141–144]. Thus, to perform a moderate model of AR, a wire thickness of ~ 0.6 mm may be more appropriate. The selective perforation of one aortic cusp caused the elevation of the ratio of heart weight to the whole body rat weight after 14 days from 2.80 to 3.37 g/kg (20%), while the perforation of two aortic cusps increased this ratio on 47% and after 30 days—on 68% [127].

Advances in Doppler echocardiographic techniques in rodents have made echocardiography a reliable tool for the diagnosing and quantification of AR [120, 122, 145]. This technique includes pulsed Doppler mapping of the depth of the regurgitated jet into LV, the slope and velocity of continuous Doppler profiles of the regurgitated jet, and color Doppler to measure cross-sectional area of the regurgitated jet relative to the cross-sectional area of the LV outflow tract (Fig. 8). From the parasternal long-axis view, the width of the LV outflow tract and the width of the color AR jet can be measured. The

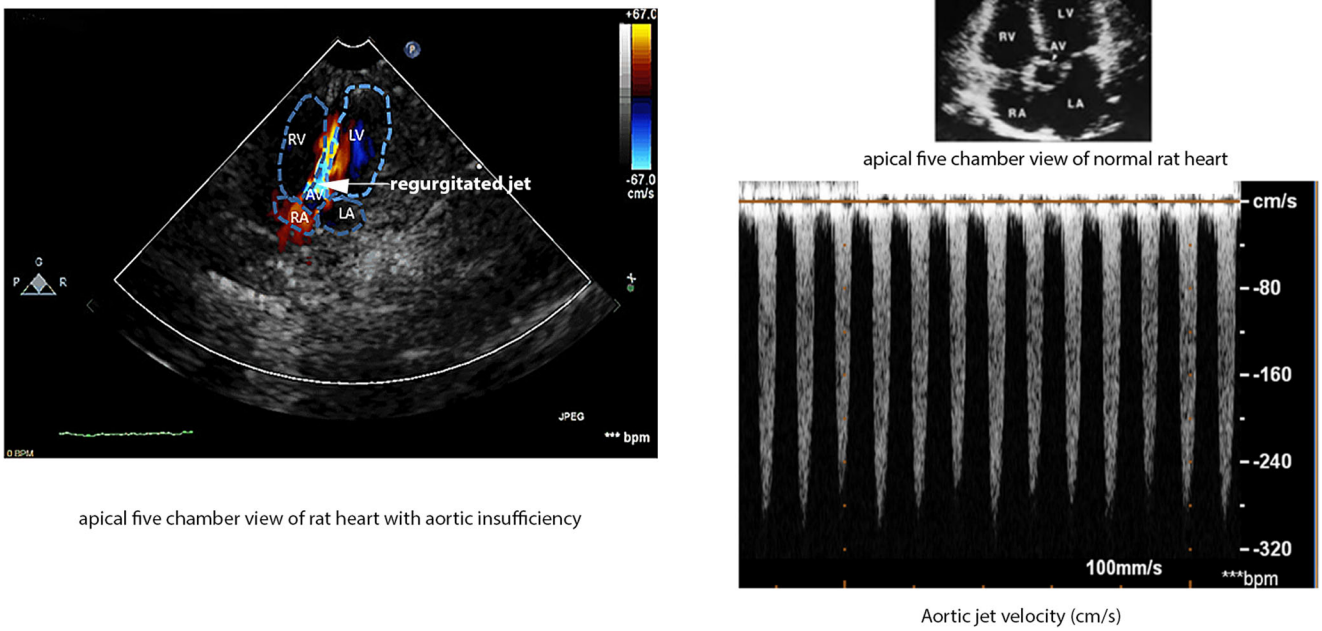

Fig. 8 Doppler echocardiography of the rat heart with aortic insufficiency. RA, right atrium; LA, left atrium; AV, aortic valve; RV, right ventricle; LV, left ventricle. Blue color indicates aortic regurgitated jet

short-axis view allows one to image the aortic valve leaflets. From the apical 4-chamber view, the AR color jet and a continuous-wave Doppler recording of the AR can be obtained. The abdominal aorta can be visualized with pulsed Doppler from the subcostal window. Abdominal aortic velocity time integrals during systole (forward flow) and diastole (reverse flow) can be obtained as well from the subcostal window [146, 147]. Aortic insufficiency is graded from 1 + to 4 + on the basis of the width of the aortic insufficiency jet. Jet width is usually normalized to LV outflow tract width. Jet width/LV outflow tract width ratio values of 0–0.26 are considered AR 1 +, 0.27–0.50 as AR 2 +, 0.51–0.70 as AR 3 +, and > 0.71 as AR 4 +. AR 3 + or 4 + is associated with holodiastolic flow reversal in the abdominal descending aorta [147]. Using Doppler echocardiography significantly decreases the mortality rate of rats with acute AR to 17% [116].

Conclusions

During the last several decades, the use of rat models to understand pathophysiological mechanisms of heart failure, identify new molecular targets, and evaluate specific therapy has proven to be invaluable. Numerous rat models for heart failure have been developed and extensively analyzed, yet have not carefully summarized practical surgical details and challenges that directly impact reproducibility. Understanding anatomy and physiology of the rat's heart and arteries, proper surgical techniques, procedural monitoring, and good postoperative care will decrease variability of results, prevent the unnecessary loss of animals, and improve overall outcomes.

Acknowledgments The authors wish to acknowledge the Gene Therapy Resource Program (GTRP). We thank Anne Olson for the excellent illustrations.

Funding information This work was supported by NIH grant 7R01 HL083078-10.

Compliance with ethical standards

Conflict of interest The authors declare that they have no conflict of interest.

Animal studies All institutional and national guidelines for the care and use of laboratory animals were followed and approved by the appropriate institutional committees. No human studies were carried out by the authors for this article.

References

1. Hongo M, Ryoke T, Ross J Jr (1997) Animal models of heart failure: recent developments and perspectives. Trends Cardiovasc Med 7(5):161–167. https://doi.org/10.1016/S1050-1738(97)00029-7
2. Patten RD, Hall-Porter MR (2009) Small animal models of heart failure: development of novel therapies, past and present. Circ Heart Fail 2(2):138–144. https://doi.org/10.1161/CIRCHEARTFAILURE.108.839761

3. Dong G-H, Xu B, Wang C-T, Qian J-J, Liu H, Huang G, Jing H (2005) A rat model of cardiopulmonary bypass with excellent survival. J Surg Res 123(2):171–175. https://doi.org/10.1016/j.jss.2004.08.007
4. Pulido JN, Neal JR, Mantilla CB, Agarwal S, Lee W-Y, Scott PD, Hubmayr RD, Zhan W-Z, Sieck GC, Farrugia G (2011) Inhaled carbon monoxide attenuates myocardial inflammatory cytokine expression in a rat model of cardiopulmonary bypass. J Extra Corpor Technol 43(3):137–143
5. Klocke R, Tian W, Kuhlmann MT, Nikol S (2007) Surgical animal models of heart failure related to coronary heart disease. Cardiovasc Res 74(1):29–38. https://doi.org/10.1016/j.cardiores.2006.11.026
6. Michael LH, Ballantyne CM, Zachariah JP, Gould KE, Pocius JS, Taffet GE, Hartley CJ, Pham TT, Daniel SL, Funk E, Entman ML (1999) Myocardial infarction and remodeling in mice: effect of reperfusion. Am J Physiol Heart Circ Physiol 277(2):H660–H668. https://doi.org/10.1152/ajpheart.1999.277.2.H660
7. Nossuli TO, Lakshminarayanan V, Baumgarten G, Taffet GE, Ballantyne CM, Michael LH, Entman ML (2000) A chronic mouse model of myocardial ischemia-reperfusion: essential in cytokine studies. Am J Physiol Heart Circ Physiol 278(4):H1049–H1055. https://doi.org/10.1152/ajpheart.2000.278.4.H1049
8. Tarnavski O (2009) Mouse surgical models in cardiovascular research. In: DiPetrillo K (ed) Cardiovascular genomics. Methods in molecular biology™ (methods and protocols), vol 573. Humana Press, New York, pp 115–137
9. Tarnavski O, McMullen JR, Schinke M, Nie Q, Kong S, Izumo S (2004) Mouse cardiac surgery: comprehensive techniques for the generation of mouse models of human diseases and their application for genomic studies. Physiol Genomics 16(3):349–360. https://doi.org/10.1152/physiolgenomics.00041.2003
10. Halpern MH (1953) The azygos vein system in the rat. Anat Rec 116(1):83–93. https://doi.org/10.1002/ar.1091160108
11. Halpern MH (1957) The dual blood supply of the rat heart. Am J Anat 101(1):1–16. https://doi.org/10.1002/aja.1001010102
12. Edvardsson N, Hirsch I, Olsson SB (1984) Right ventricular monophasic action potentials in healthy young men. Pacing Clin Electrophysiol 7(5):813–821. https://doi.org/10.1111/j.1540-8159.1984.tb05622.x
13. Varro A, Lathrop DA, Hester SB, Nanasi PP, Papp JG (1993) Ionic currents and action potentials in rabbit, rat, and Guinea pig ventricular myocytes. Basic Res Cardiol 88(2):93–102
14. Bers DM (1985) Ca influx and sarcoplasmic reticulum Ca release in cardiac muscle activation during postrest recovery. Am J Physiol Heart Circ Physiol 248(3):H366–H381. https://doi.org/10.1152/ajpheart.1985.248.3.H366
15. Lamboley CR, Murphy RM, McKenna MJ, Lamb GD (2014) Sarcoplasmic reticulum Ca2+ uptake and leak properties, and SERCA isoform expression, in type I and type II fibres of human skeletal muscle. J Physiol 592(6):1381–1395. https://doi.org/10.1113/jphysiol.2013.269373
16. Ahmed S, Rakhawy M, Abdalla A, Assaad E (1978) The comparative anatomy of the blood supply of cardiac ventricles in the albino rat and Guinea-pig. J Anat 126(Pt 1):51–57
17. Johns TN, Olson BJ (1954) Experimental myocardial infarction: I. A method of coronary occlusion in small animals. Ann Surg 140(5):675–682
18. Selye H, Bajusz E, Grasso S, Mendell P (1960) Simple techniques for the surgical occlusion of coronary vessels in the rat. Angiology 11(5):398–407. https://doi.org/10.1177/000331976001100505
19. Sievers R, Schmiedl U, Wolfe C, Moseley M, Parmley W, Brasch R, Lipton M (1989) A model of acute regional myocardial ischemia and reperfusion in the rat. Magn Reson Med 10(2):172–181. https://doi.org/10.1002/mrm.1910100203
20. Anderson PG, Bishop SP, Peterson JT (2006) Chapter 26 - cardiovascular research. In: Suckow MA, Weisbroth SH, Franklin CL (eds) The laboratory rat (second edition). Academic Press, Burlington, pp 773–802. https://doi.org/10.1016/B978-012074903-4/50029-7
21. Liu Y, Yang X-P, Nass O, Sabbah H, Peterson E, Carretero OA (1997) Chronic heart failure induced by coronary artery ligation in Lewis inbred rats. Am J Physiol Heart Circ Physiol 272(2):H722–H727. https://doi.org/10.1152/ajpheart.1997.272.2.H722
22. Cleland JGF, Torabi A, Khan NK (2005) Epidemiology and management of heart failure and left ventricular systolic dysfunction in the aftermath of a myocardial infarction. Heart 91:ii7–ii13. https://doi.org/10.1136/hrt.2005.062026
23. Maslov MY, Foianini S, Orlov MV, Januzzi JL, Lovich MA (2018) A novel paradigm for sacubitril/valsartan: beta-endorphin elevation as a contributor to exercise tolerance improvement in rats with preexisting heart failure induced by pressure overload. J Card Fail 24(11):773–782. https://doi.org/10.1016/j.cardfail.2018.10.006
24. Pfeffer MA, Pfeffer JM, Fishbein MC, Fletcher PJ, Spadaro J, Kloner RA, Braunwald E (1979) Myocardial infarct size and ventricular function in rats. Circ Res 44(4):503–512. https://doi.org/10.1161/01.RES.44.4.503
25. Pacher P, Nagayama T, Mukhopadhyay P, Bátkai S, Kass DA (2008) Measurement of cardiac function using pressure-volume conductance catheter technique in mice and rats. Nat Protoc 3(9):1422–1434. https://doi.org/10.1038/nprot.2008.138
26. Fargnoli AS, Katz MG, Williams RD, Kendle AP, Steuerwald N, Bridges CR (2016) Liquid jet delivery method featuring S100A1 gene therapy in the rodent model following acute myocardial infarction. Gene Ther 23(2):151–157. https://doi.org/10.1038/gt.2015.100
27. Hollander MR, de Waard GA, Konijnenberg LSF, Meijer-van Putten RME, van den Brom CE, Paauw N, de Vries HE, van de Ven PM, Aman J, Van Nieuw-Amerongen GP, Hordijk PL, Niessen HWM, Horrevoets AJG, Van Royen N (2016) Dissecting the effects of ischemia and reperfusion on the coronary microcirculation in a rat model of acute myocardial infarction. PLoS One 11(7):e0157233. https://doi.org/10.1371/journal.pone.0157233
28. Jakovljevic VL, Petkovic A, Bradic J, Jeremic J, Turnic TN, Srejovic I, Zivkovic V (2018) The effects of potassium-cyanide on functional recovery of isolated rat heart after ischemia and reperfusion: role of oxidative stress. Pathophysiology 25(3):177. https://doi.org/10.1016/j.pathophys.2018.07.042
29. Wayman NS, McDonald MC, Chatterjee PK, Thiemermann C (2003) Models of coronary artery occlusion and reperfusion for the discovery of novel antiischemic and antiinflammatory drugs for the heart. In: Inflammation protocols, vol 225. Humana Press, New York, pp 199–208
30. Houser SR, Margulies KB, Murphy AM, Spinale FG, Francis GS, Prabhu SD, Rockman HA, Kass DA, Molkentin JD, Sussman MA (2012) Animal models of heart failure: a scientific statement from the American Heart Association. Circ Res 111(1):131–150. https://doi.org/10.1161/RES.0b013e3182582523
31. Lindsey ML, Bolli R, JMC J, Du X-J, Frangogiannis NG, Frantz S, Gourdie RG, Holmes JW, Jones SP, Kloner RA, Lefer DJ, Liao R, Murphy E, Ping P, Przyklenk K, Recchia FA, Longacre LS, Ripplinger CM, Eyk JEV, Heusch G (2018) Guidelines for experimental models of myocardial ischemia and infarction. Am J Physiol Heart Circ Physiol 314(4):H812–H838. https://doi.org/10.1152/ajpheart.00335.2017
32. Rigalli A, Di Loreto V (2016) Experimental surgical models in the laboratory rat. CRC Press, Boca Raton
33. Motiwala SR, Gaggin HK (2016) Biomarkers to predict reverse remodeling and myocardial recovery in heart failure. Curr Heart

Fail Rep 13(5):207–218. https://doi.org/10.1007/s11897-016-0303-y
34. Golestani R, Wu C, Tio RA, Zeebregts CJ, Petrov AD, Beekman FJ, Dierckx RAJO, Boersma HH, Slart RHJA (2010) Small-animal SPECT and SPECT/CT: application in cardiovascular research. Eur J Nucl Med Mol Imaging 37(9):1766–1777. https://doi.org/10.1007/s00259-009-1321-8
35. Martinez PF, Okoshi K, Zornoff LAM, Oliveira SA, Campos DHS, Lima ARR, Damatto RL, Cezar MDM, Bonomo C, Guizoni DM, Padovani CR, Cicogna AC, Okoshi MP (2011) Echocardiographic detection of congestive heart failure in postinfarction rats. J Appl Physiol 111(2):543–551. https://doi.org/10.1152/japplphysiol.01154.2010
36. Nahrendorf M, Wiesmann F, Hiller K-H, Han H, Hu K, Waller C, Ruff J, Haase A, Ertl G, Bauer WR (2000) In vivo assessment of cardiac remodeling after myocardial infarction in rats by cine–magnetic resonance imaging. J Cardiovasc Magn Reson 2(3):171–180. https://doi.org/10.3109/10976640009146565
37. Visser EP, Disselhorst JA, Brom M, Laverman P, Gotthardt M, Oyen WJG, Boerman OC (2009) Spatial resolution and sensitivity of the Inveon small-animal PET scanner. J Nucl Med 50(1):139–147. https://doi.org/10.2967/jnumed.108.055152
38. Litwin SE, Katz SE, Morgan JP, Douglas PS (1994) Serial echocardiographic assessment of left ventricular geometry and function after large myocardial infarction in the rat. Circulation 89(1):345–354. https://doi.org/10.1161/01.CIR.89.1.345
39. Roberts CS, Maclean D, Maroko P, Kloner RA (1984) Early and late remodeling of the left ventricle after acute myocardial infarction. Am J Cardiol 54(3):407–410. https://doi.org/10.1016/0002-9149(84)90206-6
40. Yue P, Long CS, Austin R, Chang KC, Simpson PC, Massie BM (1998) Post-infarction heart failure in the rat is associated with distinct alterations in cardiac myocyte molecular phenotype. J Mol Cell Cardiol 30(8):1615–1630. https://doi.org/10.1006/jmcc.1998.0727
41. Pabis FC, Miyague NI, Francisco JC, Woitowicz V, KATd C, Faria-Neto JR, Moisés VA, Guarita-Souza LC (2008) Echocardiographic assessment of myocardial infarction evolution in young and adult rats. Arq Bras Cardiol 91(5):321–326. https://doi.org/10.1590/S0066-782X2008001700007
42. Gupta S, Prahash AJ, Anand IS (2000) Myocyte contractile function is intact in the post-infarct remodeled rat heart despite molecular alterations. Cardiovasc Res 48(1):77–88. https://doi.org/10.1016/S0008-6363(00)00160-7
43. Morgan EE, Faulx MD, McElfresh TA, Kung TA, Zawaneh MS, Stanley WC, Chandler MP, Hoit BD (2004) Validation of echocardiographic methods for assessing left ventricular dysfunction in rats with myocardial infarction. Am J Physiol Heart Circ Physiol 287(5):H2049–H2053. https://doi.org/10.1152/ajpheart.00393.2004
44. Remondino A, Rosenblatt-Velin N, Montessuit C, Tardy I, Papageorgiou I, Dorsaz P-A, Jorge-Costa M, Lerch R (2000) Altered expression of proteins of metabolic regulation during remodeling of the left ventricle after myocardial infarction. J Mol Cell Cardiol 32(11):2025–2034. https://doi.org/10.1006/jmcc.2000.1234
45. Rosenblatt-Velin N, Montessuit C, Papageorgiou I, Terrand J, Lerch R (2001) Postinfarction heart failure in rats is associated with upregulation of GLUT-1 and downregulation of genes of fatty acid metabolism. Cardiovasc Res 52(3):407–416. https://doi.org/10.1016/S0008-6363(01)00393-5
46. Ceiler DL, Nelissen-Vrancken HMG, De Mey JG, Smits JF (1998) Effect of chronic blockade of angiotensin II-receptor subtypes on aortic compliance in rats with myocardial infarction. J Cardiovasc Pharmacol 31(4):630–633. https://doi.org/10.1097/00005344-199804000-00024
47. Goldman S, Raya TE (1995) Rat infarct model of myocardial infarction and heart failure. J Card Fail 1(2):169–177. https://doi.org/10.1016/1071-9164(95)90019-5
48. Hasenfuss G (1998) Animal models of human cardiovascular disease, heart failure and hypertrophy. Cardiovasc Res 39(1):60–76. https://doi.org/10.1016/S0008-6363(98)00110-2
49. Hentschke VS, Capalonga L, Rossato DD, Perini JL, Alves JP, Quagliotto E, Stefani GP, Karsten M, Pontes M, Dal Lago P (2017) Functional capacity in a rat model of heart failure: impact of myocardial infarct size. Exp Physiol 102(11):1448–1458. https://doi.org/10.1113/EP086076
50. Takahashi M, Tanonaka K, Yoshida H, Koshimizu M, Daicho T, Oikawa R, Takeo S (2006) Possible involvement of calpain activation in pathogenesis of chronic heart failure after acute myocardial infarction. J Cardiovasc Pharmacol 47(3):413–421. https://doi.org/10.1097/01.fjc.0000210074.56614.3b
51. Fletcher PJ, Pfeffer JM, Pfeffer MA, Braunwald E (1981) Left ventricular diastolic pressure-volume relations in rats with healed myocardial infarction. Effects on systolic function. Circ Res 49(3):618–626. https://doi.org/10.1161/01.RES.49.3.618
52. Anversa P, Beghi C, Kikkawa Y, Olivetti G (1986) Myocardial infarction in rats. Infarct size, myocyte hypertrophy, and capillary growth. Circ Res 58(1):26–37. https://doi.org/10.1161/01.RES.58.1.26
53. Pfeffer MA, Pfeffer JM, Steinberg C, Finn P (1985) Survival after an experimental myocardial infarction: beneficial effects of long-term therapy with captopril. Circulation 72(2):406–412. https://doi.org/10.1161/01.CIR.72.2.406
54. Prabhu SD, Chandrasekar B, Murray DR, Freeman GL (2000) β-Adrenergic blockade in developing heart failure: effects on myocardial inflammatory cytokines, nitric oxide, and remodeling. Circulation 101(17):2103–2109. https://doi.org/10.1161/01.cir.101.17.2103
55. Minicucci MF, Gaiolla PSA, Martinez PF, Lima AR, Bonomo C, Guizoni DM, Polegato BF, Okoshi MP, Okoshi K, Matsubara BB (2011) Critical infarct size to induce ventricular remodeling, cardiac dysfunction and heart failure in rats. Int J Cardiol 151:242–243. https://doi.org/10.1016/j.ijcard.2011.06.068
56. Nozawa E, Kanashiro R, Murad N, Carvalho A, Cravo S, Campos O, Tucci PJF, Moisés VA (2006) Performance of two-dimensional Doppler echocardiography for the assessment of infarct size and left ventricular function in rats. Braz J Med Biol Res 39(5):687–695. https://doi.org/10.1590/S0100-879X2006000500016
57. Opitz CF, Mitchell GF, Pfeffer MA, Pfeffer JM (1995) Arrhythmias and death after coronary artery occlusion in the rat: continuous telemetric ECG monitoring in conscious, untethered rats. Circulation 92(2):253–261. https://doi.org/10.1161/01.CIR.92.2.253
58. Samsamshariat SA, Movahed M-R (2005) High rate of right ventricular infarction after ligation of mid left anterior descending artery in rats. Cardiovasc Revasc Med 6(1):21–23. https://doi.org/10.1016/j.carrev.2005.04.005
59. Samsamshariat SA, Samsamshariat ZA, Movahed M-R (2005) A novel method for safe and accurate left anterior descending coronary artery ligation for research in rats. Cardiovasc Revasc Med 6(3):121–123. https://doi.org/10.1016/j.carrev.2005.07.001
60. Levitt MA, Sievers RE, Wolfe CL (1994) Reduction of infarct size during myocardial ischemia and reperfusion by lazaroid U-74500A, a nonglucocorticoid 21-aminosteroid. J Cardiovasc Pharmacol 23(1):136–140. https://doi.org/10.1097/00005344-199401000-00019
61. Tang X-L, Rokosh G, Sanganalmath SK, Yuan F, Sato H, Mu J, Dai S, Li C, Chen N, Peng Y (2010) Intracoronary administration of cardiac progenitor cells alleviates left ventricular dysfunction in rats with a 30-day-old infarction. Circulation 121(2):293–305. https://doi.org/10.1161/CIRCULATIONAHA.109.871905

62. Opitz CF, Finn PV, Pfeffer MA, Mitchell GF, Pfeffer JM (1998) Effects of reperfusion on arrhythmias and death after coronary artery occlusion in the rat: increased electrical stability independent of myocardial salvage. J Am Coll Cardiol 32(1):261–267. https://doi.org/10.1016/S0735-1097(98)00173-9
63. Barrett TD, Hayes ES, Yong SL, Zolotoy AB, Abraham S, Walker MJ (2000) Ischaemia selectivity confers efficacy for suppression of ischaemia-induced arrhythmias in rats. Eur J Pharmacol 398(3): 365–374. https://doi.org/10.1016/S0014-2999(00)00295-8
64. Canyon SJ, Dobson GP (2004) Protection against ventricular arrhythmias and cardiac death using adenosine and lidocaine during regional ischemia in the in vivo rat. Am J Physiol Heart Circ Physiol 287(3):H1286–H1295. https://doi.org/10.1161/CIRCULATIONAHA.109.871905
65. Canyon SJ, Dobson GP (2006) The effect of an adenosine and lidocaine intravenous infusion on myocardial high-energy phosphates and pH during regional ischemia in the rat model in vivo. Can J Physiol Pharmacol 84(8–9):903–912. https://doi.org/10.1139/y06-035
66. Curtis M, Macleod B, Walker M (1987) Models for the study of arrhythmias in myocardial ischaemia and infarction: the use of the rat. J Mol Cell Cardiol 19(4):399–419. https://doi.org/10.1016/S0022-2828(87)80585-0
67. Bergey JL, Nocella K, McCallum JD (1982) Acute coronary artery occlusion-reperfusion-induced arrhythmias in rats, dogs and pigs: antiarrhythmic evaluation of quinidine, procainamide and lidocaine. Eur J Pharmacol 81(2):205–216. https://doi.org/10.1016/0014-2999(82)90438-1
68. Johnston K, MacLeod B, Walker M (1983) Responses to ligation of a coronary artery in conscious rats and the actions of antiarrhythmics. Can J Physiol Pharmacol 61(11):1340–1353. https://doi.org/10.1139/y83-193
69. Marshall R, Muir A, WINSLOW E (1982) The effects of postligation administration of org 6001 and disopyramide on early ischaemia-induced arrhythmias in the anaesthetized rat. Br J Pharmacol 76(4):501–503. https://doi.org/10.1111/j.1476-5381.1982.tb09245.x
70. Agelaki MG, Pantos C, Korantzopoulos P, Tsalikakis DG, Baltogiannis GG, Fotopoulos A, Kolettis TM (2007) Comparative antiarrhythmic efficacy of amiodarone and dronedarone during acute myocardial infarction in rats. Eur J Pharmacol 564(1–3):150–157. https://doi.org/10.1016/j.ejphar.2007.02.052
71. Kolettis TM, Agelaki MG, Baltogiannis GG, Vlahos AP, Mourouzis I, Fotopoulos A, Pantos C (2007) Comparative effects of acute vs. chronic oral amiodarone treatment during acute myocardial infarction in rats. Europace 9(11):1099–1104. https://doi.org/10.1093/europace/eum196
72. Au T, Curtis M, Walker M (1987) Effects of (-),(+/-), and (+) verapamil on coronary occlusion-induced mortality and infarct size. J Cardiovasc Pharmacol 10(3):327–331. https://doi.org/10.1097/00005344-198709000-00012
73. Curtis M, Walker M, Yuswack T (1986) Actions of the verapamil analogues, anipamil and ronipamil, against ischaemia-induced arrhythmias in conscious rats. Br J Pharmacol 88(2):355–361. https://doi.org/10.1111/j.1476-5381.1986.tb10211.x
74. Kinoshita K, Mitani A, Hearse DJ, Braimbridge MV, Manning AS (1989) Reperfusion-induced arrhythmias in the conscious rat: a comparative study with three calcium antagonists. J Surg Res 47(2):166–172. https://doi.org/10.1016/0022-4804(89)90083-8
75. Hock CE, Beck LD, Bodine RC, Reibel DK (1990) Influence of dietary n-3 fatty acids on myocardial ischemia and reperfusion. Am J Physiol Heart Circ Physiol 259(5):H1518–H1526. https://doi.org/10.1152/ajpheart.1990.259.5.H1518
76. Jeuthe S, Dietrich T, Berger F, Kuehne T, Kozerke S, Messroghli DR (2015) Closed-chest small animal model to study myocardial infarction in an MRI environment in real time. Int J Cardiovasc Imaging 31(1):115–121. https://doi.org/10.1007/s10554-014-0539-0
77. Barbosa ME, Alenina N, Bader M (2005) Induction and analysis of cardiac hypertrophy in transgenic animal models. In: Molecular cardiology. Humana Press, New York, pp 339–352
78. Feldman AM, Weinberg EO, Ray PE, Lorell BH (1993) Selective changes in cardiac gene expression during compensated hypertrophy and the transition to cardiac decompensation in rats with chronic aortic banding. Circ Res 73(1):184–192. https://doi.org/10.1161/01.RES.73.1.184
79. Litwin SE, Katz SE, Weinberg EO, Lorell BH, Aurigemma GP, Douglas PS (1995) Serial echocardiographic-Doppler assessment of left ventricular geometry and function in rats with pressure-overload hypertrophy: chronic angiotensin-converting enzyme inhibition attenuates the transition to heart failure. Circulation 91(10):2642–2654. https://doi.org/10.1161/01.cir.89.1.345
80. Zaha V, Grohmann J, Göbel H, Geibel A, Beyersdorf F, Doenst T (2003) Experimental model for heart failure in rats-induction and diagnosis. Thorac Cardiovasc Surg 51(04):211–215. https://doi.org/10.1055/s-2003-42264
81. Boluyt MO, Robinson KG, Meredith AL, Sen S, Lakatta EG, Crow MT, Brooks WW, Conrad CH, Bing OH (2005) Heart failure after long-term supravalvular aortic constriction in rats. Am J Hypertens 18(2):202–212. https://doi.org/10.1016/j.amjhyper.2004.08.034
82. Turcani M, Rupp H (2000) Heart failure development in rats with ascending aortic constriction and angiotensin-converting enzyme inhibition. Br J Pharmacol 130(7):1671–1677. https://doi.org/10.1038/sj.bjp.0703467
83. Miyamoto MI, Del Monte F, Schmidt U, DiSalvo TS, Kang ZB, Matsui T, Guerrero JL, Gwathmey JK, Rosenzweig A, Hajjar RJ (2000) Adenoviral gene transfer of SERCA2a improves left-ventricular function in aortic-banded rats in transition to heart failure. Proc Natl Acad Sci U S A 97(2):793–798. https://doi.org/10.1073/pnas.97.2.793
84. Nair K, Cutilletta A, Zak R, Koide T, Rabinowitz M (1968) Biochemical correlates of cardiac hypertrophy: I. Experimental model; changes in heart weight, RNA content, and nuclear RNA polymerase activity. Circ Res 23(3):451–462. https://doi.org/10.1161/01.RES.23.3.451
85. Schunkert H, Dzau V, Tang SS, Hirsch A, Apstein C, Lorell B (1990) Increased rat cardiac angiotensin converting enzyme activity and mRNA expression in pressure overload left ventricular hypertrophy. Effects on coronary resistance, contractility, and relaxation. J Clin Invest 86(6):1913–1920. https://doi.org/10.1172/JCI114924
86. Weinberg EO, Schoen FJ, George D, Kagaya Y, Douglas PS, Litwin SE, Schunkert H, Benedict CR, Lorell BH (1994) Angiotensin-converting enzyme inhibition prolongs survival and modifies the transition to heart failure in rats with pressure overload hypertrophy due to ascending aortic stenosis. Circulation 90(3):1410–1422. https://doi.org/10.1161/01.CIR.90.3.1410
87. Cantor EJ, Babick AP, Vasanji Z, Dhalla NS, Netticadan T (2005) A comparative serial echocardiographic analysis of cardiac structure and function in rats subjected to pressure or volume overload. J Mol Cell Cardiol 38(5):777–786. https://doi.org/10.1016/j.yjmcc.2005.02.012
88. Ku H-C, Su M-J (2014) DPP4 deficiency preserved cardiac function in abdominal aortic banding rats. PLoS One 9(1):e85634. https://doi.org/10.1371/journal.pone.0085634
89. Braun MU, Szalai P, Strasser RH, Borst MM (2003) Right ventricular hypertrophy and apoptosis after pulmonary artery banding: regulation of PKC isozymes. Cardiovasc Res 59(3): 658–667. https://doi.org/10.1016/S0008-6363(03)00470-X

90. Faber MJ, Dalinghaus M, Lankhuizen IM, Steendijk P, Hop WC, Schoemaker RG, Duncker DJ, Lamers JM, Helbing WA (2006) Right and left ventricular function after chronic pulmonary artery banding in rats assessed with biventricular pressure-volume loops. Am J Physiol Heart Circ Physiol 291(4):H1580–H1586. https://doi.org/10.1152/ajpheart.00286.2006
91. Fujimoto Y, Urashima T, Shimura D, Ito R, Kawachi S, Kajimura I, Akaike T, Kusakari Y, Fujiwara M, Ogawa K (2016) Low cardiac output leads hepatic fibrosis in right heart failure model rats. PLoS One 11(2):e0148666. https://doi.org/10.1371/journal.pone.0148666
92. Hirata M, Ousaka D, Arai S, Okuyama M, Tarui S, Kobayashi J, Kasahara S, Sano S (2015) Novel model of pulmonary artery banding leading to right heart failure in rats. Biomed Res Int 2015:1–10. https://doi.org/10.1155/2015/753210
93. Hoashi T, Matsumiya G, Miyagawa S, Ichikawa H, Ueno T, Ono M, Saito A, Shimizu T, Okano T, Kawaguchi N (2009) Skeletal myoblast sheet transplantation improves the diastolic function of a pressure-overloaded right heart. J Thorac Cardiovasc Surg 138(2):460–467. https://doi.org/10.1016/j.jtcvs.2009.02.018
94. Bogaard HJ, Natarajan R, Henderson SC, Long CS, Kraskauskas D, Smithson L, Ockaili R, McCord JM, Voelkel NF (2009) Chronic pulmonary artery pressure elevation is insufficient to explain right heart failure. Circulation 120(20):1951–1960. https://doi.org/10.1161/CIRCULATIONAHA.109.883843
95. Zierhut W, Zimmer H, Gerdes A (1990) Influence of ramipril on right ventricular hypertrophy induced by pulmonary artery stenosis in rats. J Cardiovasc Pharmacol 16(3):480–486
96. Opie LH, Commerford PJ, Gersh BJ, Pfeffer MA (2006) Controversies in ventricular remodelling. Lancet 367(9507):356–367. https://doi.org/10.1016/S0140-6736(06)68074-4
97. Drazner MH (2011) The progression of hypertensive heart disease. Circulation 123(3):327–334. https://doi.org/10.1161/CIRCULATIONAHA.108.845792
98. Del Monte F, Butler K, Boecker W, Gwathmey JK, Hajjar RJ (2002) Novel technique of aortic banding followed by gene transfer during hypertrophy and heart failure. Physiol Genomics 9(1):49–56. https://doi.org/10.1152/physiolgenomics.00035.2001
99. Bregagnollo EA, Mestrinel MA, Okoshi K, Carvalho FC, Bregagnollo IF, Padovani CR, Cicogna AC (2007) Relative role of left ventricular geometric remodeling and of morphological and functional myocardial remodeling in the transition from compensated hypertrophy to heart failure in rats with supravalvar aortic stenosis. Arq Bras Cardiol 88(2):225–233. https://doi.org/10.1590/S0066-782X2007000200015
100. Chaanine AH, Hajjar RJ (2018) Characterization of the differential progression of left ventricular remodeling in a rat model of pressure overload induced heart failure. Does clip size matter?. In: Ishikawa K (eds) Experimental models of cardiovascular diseases. Methods in molecular biology, vol 1816. Humana Press, New York, pp 195–206
101. Chaanine AH, Sreekumaran Nair K, Bergen RH III, Klaus K, Guenzel AJ, Hajjar RJ, Redfield MM (2017) Mitochondrial integrity and function in the progression of early pressure overload–induced left ventricular remodeling. J Am Heart Assoc 6(6):e005869. https://doi.org/10.1161/JAHA.117.005869
102. Ajith Kumar G, Binil Raj SKS, Sanjay G (2014) Ascending aortic constriction in rats for creation of pressure overload cardiac hypertrophy model. J Vis Exp (88). https://doi.org/10.3791/50983
103. Turcani M, Rupp H (1997) Etomoxir improves left ventricular performance of pressure-overloaded rat heart. Circulation 96(10):3681–3686. https://doi.org/10.1161/01.cir.96.10.3681
104. Seymour A-ML, Giles L, Ball V, Miller JJ, Clarke K, Carr CA, Tyler DJ (2015) In vivo assessment of cardiac metabolism and function in the abdominal aortic banding model of compensated cardiac hypertrophy. Cardiovasc Res 106(2):249–260. https://doi.org/10.1093/cvr/cvv101
105. Pires MD, Salemi VM, Cestari IA, Picard MH, Leirner AA, Mady C, Cestari IN (2003) Noninvasive assessment of hemodynamic parameters in experimental stenosis of the ascending aorta. Artif Organs 27(8):695–700. https://doi.org/10.1046/j.1525-1594.2003.07276.x
106. Salemi VM, Pires MD, Cestari IN, Cestari IA, Picard MH, Leirner AA, Mady C (2004) Echocardiographic assessment of global ventricular function using the myocardial performance index in rats with hypertrophy. Artif Organs 28(4):332–337. https://doi.org/10.1111/j.1525-1594.2004.47350.x
107. Shingu Y, Amorim PA, Nguyen TD, Osterholt M, Schwarzer M, Doenst T (2013) Echocardiography alone allows the determination of heart failure stages in rats with pressure overload. Thorac Cardiovasc Surg 61(08):718–725. https://doi.org/10.1055/s-0032-1326775
108. Slama M, Ahn J, Varagic J, Susic D, Frohlich ED (2004) Long-term left ventricular echocardiographic follow-up of SHR and WKY rats: effects of hypertension and age. Am J Physiol Heart Circ Physiol 286(1):H181–H185. https://doi.org/10.1152/ajpheart.00642.2003
109. Higuchi T, Nekolla SG, Jankaukas A, Weber AW, Huisman MC, Reder S, Ziegler SI, Schwaiger M, Bengel FM (2007) Characterization of Normal and infarcted rat myocardium using a combination of small-animal PET and clinical MRI. J Nucl Med 48(2):288–294
110. Vanhoutte L, Gerber BL, Gallez B, Po C, Magat J, Jean-Luc B, Feron O, Moniotte S (2016) High field magnetic resonance imaging of rodents in cardiovascular research. Basic Res Cardiol 111(4):46. https://doi.org/10.1007/s00395-016-0565-2
111. Songstad NT, Johansen D, How O-J, Kaaresen PI, Ytrehus K, Acharya G (2014) Effect of transverse aortic constriction on cardiac structure, function and gene expression in pregnant rats. PLoS One 9(2):e89559. https://doi.org/10.1371/journal.pone.0089559
112. Lygate CA, Schneider JE, Hulbert K, ten Hove M, Sebag-Montefiore LM, Cassidy PJ, Clarke K, Neubauer S (2006) Serial high resolution 3D–MRI after aortic banding in mice: band internalization is a source of variability in the hypertrophic response. Basic Res Cardiol 101(1):8–16. https://doi.org/10.1007/s00395-005-0546-3
113. Jalal Z, Roubertie F, Fournier E, Dubes V, Benoist D, Naulin J, Delmond S, Durand M, Haissaguerre M, Bernus O (2017) Unexpected internalization of a pulmonary artery band in a porcine model of Tetralogy of Fallot. World J Pediatr Congenit Heart Surg 8(1):48–54. https://doi.org/10.1177/2150135116668828
114. Mann DL, Barger PM, Burkhoff D (2012) Myocardial recovery and the failing heart: myth, magic, or molecular target? J Am Coll Cardiol 60(24):2465–2472. https://doi.org/10.1016/j.jacc.2012.06.062
115. Brower GL, Janicki JS (2001) Contribution of ventricular remodeling to pathogenesis of heart failure in rats. Am J Physiol Heart Circ Physiol 280(2):H674–H683. https://doi.org/10.1152/ajpheart.2001.280.2.H674
116. Arsenault M, Plante E, Drolet M-C, Couet J (2002) Experimental aortic regurgitation in rats under echocardiographic guidance. J Heart Valve Dis 11(1):128–134
117. Chancey AL, Brower GL, Peterson JT, Janicki JS (2002) Effects of matrix metalloproteinase inhibition on ventricular remodeling due to volume overload. Circulation 105(16):1983–1988. https://doi.org/10.1161/01.cir.0000014686.73212.da
118. Gerdes A, Campbell S, Hilbelink D (1988) Structural remodeling of cardiac myocytes in rats with arteriovenous fistulas. Lab Investig 59(6):857–861. https://doi.org/10.1161/01.CIR.86.2.426

119. Mickle JP, Menges JT, Day AL, Quisling R, Ballinger W (1981) Experimental aortocaval fistulae in rats. Microsurgery 2(4):283–288. https://doi.org/10.1002/micr.1920020410
120. Munakata H, Assmann A, Poudel-Bochmann B, Horstkötter K, Kamiya H, Okita Y, Lichtenberg A, Akhyari P (2013) Aortic conduit valve model with controlled moderate aortic regurgitation in rats. Circ J 77(9):2295–2302. https://doi.org/10.1253/circj.CJ-12-1439
121. Ocampo C, Ingram P, Ilbawi M, Arcilla R, Gupta M (2003) Revisiting the surgical creation of volume load by aorto-caval shunt in rats. Mol Cell Biochem 251(1–2):139–143. https://doi.org/10.1016/S0022-2828(01)90340-2
122. Plante E, Couet J, Gaudreau M, Dumas M-P, Drolet M-C, Arsenault M (2003) Left ventricular response to sustained volume overload from chronic aortic valve regurgitation in rats. J Card Fail 9(2):128–140. https://doi.org/10.1054/jcaf.2003.17
123. Su X, Brower G, Janicki JS, Chen Y-F, Oparil S, Dell'Italia LJ (1999) Differential expression of natriuretic peptides and their receptors in volume overload cardiac hypertrophy in the rat. J Mol Cell Cardiol 31(10):1927–1936. https://doi.org/10.1006/jmcc.1999.1025
124. Wei C-C, Lucchesi PA, Tallaj J, Bradley WE, Powell PC, Dell'Italia LJ (2003) Cardiac interstitial bradykinin and mast cells modulate pattern of LV remodeling in volume overload in rats. Am J Physiol Heart Circ Physiol 285(2):H784–H792. https://doi.org/10.1152/ajpheart.00793.2001
125. Wu J, Cheng Z, Gu Y, Zou W, Zhang M, Zhu P, Hu S (2015) Aggravated cardiac remodeling post aortocaval fistula in unilateral nephrectomized rats. PLoS One 10(8):e0134579. https://doi.org/10.1371/journal.pone.0134579
126. Isoyama S, Grossman W, Wei JY (1988) Effect of age on myocardial adaptation to volume overload in the rat. J Clin Invest 81(6):1850–1857. https://doi.org/10.1172/JCI113530
127. Toshihiko U, Tamahito Y, Hiroyuki M, Yujiro H, Mitsuyoshi N (1989) A simple method for producing graded aortic insufficiencies in rats and subsequent development of cardiac hypertrophy. J Pharmacol Methods 22(4):249–257. https://doi.org/10.1016/0160-5402(89)90004-1
128. Maslov MY, Foianini S, Mayer D, Orlov MV, Lovich MA (2018) Synergy between sacubitril and valsartan leads to hemodynamic, antifibrotic, and exercise tolerance benefits in rats with preexisting heart failure. Am J Physiol Heart Circ Physiol 316(2):H289–H297. https://doi.org/10.1152/ajpheart.00579.2018
129. Desjardins S, Mueller RW, Cauchy MJ (1988) A pressure overload model of congestive heart failure in rats. Cardiovasc Res 22(10):696–702. https://doi.org/10.1093/cvr/22.10.696
130. Huang M, LeBlanc MH, Hester RL (1994) Evaluation of the needle technique for producing an arteriovenous fistula. J Appl Physiol 77(6):2907–2911. https://doi.org/10.1152/jappl.1994.77.6.2907
131. Liu Z, Hilbelink DR, Crockett WB, Gerdes AM (1991) Regional changes in hemodynamics and cardiac myocyte size in rats with aortocaval fistulas. 1. Developing and established hypertrophy. Circ Res 69(1):52–58. https://doi.org/10.1161/01.RES.69.1.52
132. Wang X, Ren B, Liu S, Sentex E, Tappia PS, Dhalla NS (2003) Characterization of cardiac hypertrophy and heart failure due to volume overload in the rat. J Appl Physiol 94(2):752–763. https://doi.org/10.1152/japplphysiol.00248.2002
133. Wu J, Cheng Z, Zhang M, Zhu P, Gu Y (2016) Impact of aortocaval shunt flow on cardiac and renal function in unilateral nephrectomized rats. Sci Rep 6:27493. https://doi.org/10.1038/srep27493
134. Langer S, Heiss C, Paulus N, Bektas N, Mommertz G, Rowinska Z, Westenfeld R, Jacobs MJ, Fries M, Koeppel TA (2009) Functional and structural response of arterialized femoral veins in a rodent AV fistula model. Nephrol Dial Transplant 24(7):2201–2206. https://doi.org/10.1093/ndt/gfp033
135. Kraiss LW, Kirkman TR, Kohler TR, Zierler B, Clowes AW (1991) Shear stress regulates smooth muscle proliferation and neointimal thickening in porous polytetrafluoroethylene grafts. Arterioscler Thromb 11(6):1844–1852. https://doi.org/10.1161/01.ATV.11.6.1844
136. Manning E, Skartsis N, Orta AM, Velazquez OC, Liu Z-J, Asif A, Salman LH, Vazquez-Padron RI (2012) A new arteriovenous fistula model to study the development of neointimal hyperplasia. J Vasc Res 49(2):123–131. https://doi.org/10.1159/000332327
137. Flaim SF, Minteer WJ, Nellis SH, Clark DP (1979) Chronic arteriovenous shunt: evaluation of a model for heart failure in rat. Am J Physiol Heart Circ Physiol 236(5):H698–H704. https://doi.org/10.1152/ajpheart.1979.236.5.H698
138. Stark RJ, Shekerdemian LS (2013) Estimating intracardiac and extracardiac shunting in the setting of complex congenital heart disease. Ann Pediatr Cardiol 6(2):145–151. https://doi.org/10.4103/0974-2069.115259
139. Linardi D, Rungatscher A, Morjan M, Marino P, Luciani GB, Mazzucco A, Faggian G (2014) Ventricular and pulmonary vascular remodeling induced by pulmonary overflow in a chronic model of pretricuspid shunt. J Thorac Cardiovasc Surg 148(6):2609–2617. https://doi.org/10.1016/j.jtcvs.2014.04.044
140. Garcia R, Diebold S (1990) Simple, rapid, and effective method of producing aortocaval shunts in the rat. Cardiovasc Res 24(5):430–432. https://doi.org/10.1093/cvr/24.5.430
141. Kimura M, Umemura K, Ohashi K, Nakashima M (1998) Effect of ecadotril, a neutral endopeptidase inhibitor, on myocardial hypertrophy in the rat aortic insufficiency model. Can J Cardiol 14(1):63–68
142. Légaré J-F, Nanton MA, Bryan P, Lee TDG, Ross DB (2000) Aortic valve graft implantation in rats: a new functional model. J Thorac Cardiovasc Surg 120(4):679–685. https://doi.org/10.1067/mtc.2000.109239
143. Légaré J-F, Ross DB (2004) Suggestion for functional model to test effects of decellularization of rat aortic valve allografts on leaflet destruction and extracellular matrix remodeling. J Thorac Cardiovasc Surg 128(1):155–156. https://doi.org/10.1016/j.jtcvs.2004.03.015
144. Morita H, Tanaka I, Oda T, Ichiyama A, Yamazaki T, Uematsu T, Nakashima M, Yoshimi T (1990) Atrial natriuretic peptide messenger RNA and peptide in rats with aortic valve insufficiency. Peptides 11(4):843–847. https://doi.org/10.1016/0196-9781(90)90202-G
145. Koike MK, Matsubara BB, Matsubara LS, Frimm CC (2014) Sequential hemodynamic assessment in aortic valve insufficiency in rats. Med Express 1:214–218
146. Chen M, Luo H, Miyamoto T, Atar S, Kobal S, Rahban M, Brasch AV, Makkar R, Neuman Y, Naqvi TZ, Tolstrup K, Siegel RJ (2003) Correlation of echo-Doppler aortic valve regurgitation index with angiographic aortic regurgitation severity. Am J Cardiol 92(5):634–635. https://doi.org/10.1016/S0002-9149(03)00743-4
147. Tani LY, Minich LL, Day RW, Orsmond GS, Shaddy RE (1997) Doppler evaluation of aortic regurgitation in children. Am J Cardiol 80(7):927–931. https://doi.org/10.1016/S0002-9149(97)00547-X